[redacted]

Copy 202
RM E53L16

NACA

RESEARCH MEMORANDUM

INVESTIGATION OF THRUST AND DRAG CHARACTERISTICS OF A PLUG-TYPE EXHAUST NOZZLE

By Donald P. Hearth and Gerald C. Gorton

Lewis Flight Propulsion Laboratory
Cleveland, Ohio

CLASSIFIED DOCUMENT

NATIONAL ADVISORY COMMITTEE
FOR AERONAUTICS

WASHINGTON

February 19, 1954

[redacted]

NACA RM E53L16

NATIONAL ADVISORY COMMITTEE FOR AERONAUTICS

RESEARCH MEMORANDUM

INVESTIGATION OF THRUST AND DRAG CHARACTERISTICS OF A PLUG-TYPE EXHAUST NOZZLE

By Donald P. Hearth and Gerald C. Gorton

SUMMARY

An investigation was conducted in the 8- by 6-foot supersonic wind tunnel on the external and internal characteristics of a plug-type exhaust nozzle. Two positions of the center plug, one simulating a convergent nozzle and the other a convergent-divergent nozzle, were investigated. Data were obtained at free-stream Mach numbers of 0.1, 0.6, 1.6, and 2.0 over a pressure-ratio range of 1 to 20 and angles of attack of zero and 8°.

Results of this investigation indicated that the plug nozzle had thrust-minus-drag performance over the entire pressure-ratio range comparable with equivalent conventional nozzles. The effect of the exhaust jet on the external aerodynamics was similar to results observed for conventional nozzles. In addition, the thrust characteristics were generally insensitive to external flow and good agreement was noted with data obtained on comparable plug nozzles in quiescent air.

INTRODUCTION

Supersonic jet-engine operation requires that the exhaust nozzle for such engines be operated over a range of pressure ratios. Moreover, for a turbojet engine equipped with afterburner, for example, throat-area variation may also be desired. Numerous forms of variable-geometry nozzles have been proposed for jet-engine application, and preliminary evaluation of several practical designs has been made in quiescent air (refs. 1 to 4).

One of the more promising variable-geometry nozzles is the plug type (refs. 3 to 5), which utilizes axial translation of a streamlined centerbody to achieve a variation both in the minimum area and in the expansion ratio. Although the plug nozzle does not offer an independent variation of these two quantities, it may be designed to satisfy a desired throat-area variation with expansion-ratio change. If not

designed to satisfy conditions over an entire schedule, a plug nozzle may at least have applications as a two-position device such as for afterburner off and on operation.

In order to fully evaluate exhaust nozzles, the effect of external flow on the internal nozzle thrust characteristics, as well as the effect of the jet on external aerodynamics, is required. A comprehensive program has therefore been undertaken in the NACA Lewis 8- by 6-foot supersonic wind tunnel. Investigated as a part of this program was a plug-type exhaust nozzle installed on a generalized NACA jet-exit model. Two positions of the center plug simulating the two end points of a throat-area - expansion ratio schedule were investigated. In one position the nozzle was physically a convergent-divergent nozzle, while in the other position the nozzle was physically a convergent nozzle. Thrust and drag characteristics are presented for free-stream Mach numbers of 0.1, 0.6, 1.6, and 2.0 at zero angle of attack over a pressure-ratio range from 1 to 20. Some internal data are also presented at angles of attack of 8°. All data were obtained with a jet temperature of 400° F.

APPARATUS AND PROCEDURE

Installation

The generalized exit model on which the plug nozzle was investigated is shown installed in the 8- by 6-foot supersonic wind tunnel in figures 1 and 2. The model was supported by two 11-percent-thick horizontal struts of circular-arc cross section. These struts were attached to trunnions mounted in the tunnel wall and were rotated to vary the model angle of attack.

The source of the model internal air flow was a separately controlled air supply. Air flow was measured with a sharp-edge orifice, and the internal model pressure was varied with a butterfly valve located downstream of the orifice (fig. 1). In order to avoid the possibility of condensation shocks in the nozzle, the air was preheated to a temperature of 400° F by means of a conventional turbojet can combustor. Air was introduced into the model through the hollow support struts as indicated in figure 1.

Basic Exit Model and Data Reduction

The basic model, shown schematically in figure 3, consisted of three main components: an outer shell, the "capsule," and an inner liner. The axially symmetric nose section of the outer shell was of parabolic contour based on the following equation (x is the axial distance from the nose tip and y the distance from the model axis):

$$y = 4\frac{1}{8}\left[1 - \left(\frac{40 - x}{40}\right)^2\right]$$

The parabolic contour extended to a body diameter of $8\frac{1}{4}$ inches at a point 40 inches from the nose. This diameter was maintained for the next 31.60 inches, and a suitable afterbody for the nozzle was added beyond the cylindrical section.

3138

As can be seen from figure 3, the two support struts, through which air was brought into the model, were rigidly attached to the capsule. A turn of 90° was required for the air to flow axially through the model. Since the internal air flow was confined to the capsule and inner liner (maximum internal diameter of 7.0 in.), the external forces were applied only on the outer shell while the internal forces were applied on the capsule and inner liner.

CH-1 back

A strain-gage balance located in the nose ahead of the capsule was used to obtain force measurements. In order to separate the internal and external forces, two runs, each with a different balance connection (figs. 3(a) and (b)), were required. The "drag" connection (fig. 3(a)) was such that only the forces on the outer shell were applied to the balance, and total external drag could then be obtained. The "thrust-minus-drag" connection (fig. 3(b)) was such that both the inner liner and the outer shell were restrained by the balance; thus, the sum of the external and the internal forces on these surfaces was measured. The internal forces were equivalent to the change in internal axial momentum from the inner-liner entrance (station 2) to the nozzle exit (station 4). Since calibration indicated that the air entering the capsule had no component in the axial direction, the momentum at station 2 was assumed equal to the net internal axial force acting on the capsule. The thrust-minus-drag connection, therefore, yielded the jet thrust minus the total external drag of the model. The details of utilizing the balance readings (symbols defined in appendix A) in obtaining these forces are discussed in appendix B. Adding the external drag force to the measured thrust-minus-drag force yielded the jet thrust of the nozzle. This measured jet thrust was compared with an ideal jet thrust defined as the product of the actual mass flow and the exit velocity corresponding to complete isentropic expansion (see appendix B). The nozzle mass-flow coefficient is defined as the ratio of actual to ideal mass flow passed through the nozzle and was calculated as shown in appendix B. Air flow and preheater fuel flow were measured with an A.S.M.E. orifice and a rotameter, respectively. Additional data obtained included static pressures on the plug, boattail, and base. The instrumentation was located on the top and bottom and also on one side of the plug and boattail as shown in figure 4.

Plug-Nozzle Configuration

The exhaust-nozzle configuration investigated consisted of an internally located plug supported by four struts within a parabolic-shaped boattail. Coordinates of the plug, obtained from the lemniscate of Bernoulli's equation modified for a fineness ratio of 3.0, are presented in table I. Also included in the table are the inner-liner coordinates. The external afterbody, which was connected to the cylindrical section of the basic model at station 71.60, was cylindrical for 3.85 inches and terminated with a parabolic-shaped boattail, the equation for which is indicated in figure 4.

The two plug positions investigated are shown in figure 4 (see fig. 5 for the variation in flow areas). The convergent-divergent position was such that the end of the plug coincided with the end of the afterbody at station 83.75. This configuration corresponded to a convergent-divergent nozzle with a design pressure ratio of 5.8 and a throat area of 0.140 square foot. The other position of the plug was such that the throat area of 0.090 square foot occurred at the end of the afterbody. With the plug in the latter position, the nozzle was physically convergent except for the protruding section of the plug. These two plug positions were designed to simulate the two end points of a variable-throat-area nozzle which, for example, would be required with an afterburner-temperature-ratio variation from 1.0 to 2.4.

RESULTS AND DISCUSSION

External Characteristics

The effect of the jet issuing from the plug nozzle on the boattail pressure distribution is presented in figure 6. Although data are presented only at a free-stream Mach number of 2.0, the trends noted were also obtained at the other Mach numbers investigated. The variation in pressure coefficient $C_{p,a}$ is presented as a function of nozzle pressure ratio such that a negative value of pressure coefficient indicates a drag force while a positive value represents a thrust force. As can be seen from figure 6(a), when the plug was in the convergent-divergent position, the boattail pressures were affected only slightly by the nozzle pressure ratio. However, with the plug in the convergent position (fig. 6(b)), a considerably greater influence of the jet pressure ratio on the boattail pressures was noted (pressures were influenced upstream as much as 0.6 of the jet diameter). These same trends have been noted for conventional nozzles (ref. 6) and are caused by the degree of nozzle underexpansion, especially noticeable with convergent nozzles. Because of the off-design operation of the nozzle, however, a large loss in thrust occurs concurrent with this drag reduction for conventional nozzle types.

Presented in figure 7 is the variation of the boattail pressure-drag coefficient $C_{D,a}$ (based on maximum cross-sectional area of the body) with the nozzle pressure ratio for free-stream Mach numbers of 2.0, 1.6, and 0.6. Data are presented for both plug positions and were obtained from integration of boattail pressure distributions such as shown in figure 6.

As expected from the pressure distributions, the boattail pressure drag with the plug in the convergent-divergent position (fig. 7(a)) was virtually unaffected by nozzle pressure ratio even at pressure ratios in excess of the design value of 5.8. Included on the figure for comparison purposes is the boattail pressure-drag variation at a Mach number of 2.0 of a conventional convergent-divergent nozzle. For the conventional nozzle the boattail drag decreased at pressure ratios above the design value (5.3). This difference in trends may be due in part to the difference in flow angles (both internal and external) in the plane at which the boattail terminates. If two nozzles are to be considered for the same engine operating point, the throat areas would have to be the same. Since the throat areas for the two nozzles shown on figure 7(a) were different, a comparison of absolute values of boattail drag is not made.

With the plug in the convergent position, the boattail pressure drag (fig. 7(b)) was reduced by the jet issuing from the nozzle for pressure ratios in excess of 4 to 5 supersonically and for all pressure ratios with subsonic external flow. Included in this figure is the boattail drag variation at a Mach number of 2.0 for a conventional convergent nozzle. As shown for comparable Mach numbers, the drag reduction for the conventional nozzle occurred at lower values of nozzle pressure ratio than for the plug nozzle shown. In addition to a difference in the flow angles, it should be pointed out that part of the expansion of the flow from the throat of the plug nozzle occurred toward the center of the jet, thereby tending to reduce the growth of the jet. Since both the conventional convergent and the convergent plug nozzles had the same throat areas, a comparison of the absolute values of boattail pressure drag is permissible. Because of the area occupied by the plug itself, the projected afterbody area was less than that required by a conventional convergent nozzle. As expected, therefore, the values of boattail pressure drag were appreciably lower for the plug nozzle.

The nature of the jet influence on the boattail aerodynamics is apparent from the schlieren photographs presented in figure 8. (It should be noted that the dark horizontal strip near the center of the jet is the upper half of the wake from the horizontal support struts.) Photographs at low and high pressure ratios for a Mach number of 2.0 are presented for the convergent-divergent plug position (figs. 8(a) and (b)) and for the convergent plug position (figs. 8(c) and (d)). A large change in nozzle pressure ratio caused very little movement of the

trailing shock with the plug in the convergent-divergent position but a large movement of the trailing shock with the plug in the convergent plug position. This trailing shock (ref. 6) was caused by the interaction of the jet and the external stream and appears near the body as a series of compression waves due to thickening of the body boundary layer. The movement of this shock was primarily responsible for the change in the boattail pressure distributions and drag variations presented in figures 6 and 7. However, it should be noted that the trailing shock moved only about half the distance upstream, as did the observed pressure feedback through the boundary layer (fig. 6).

In order to maintain free relative movement between the inner liner and the outer shell, a clearance between these components was allowed. This clearance resulted in an appreciable base area. Influence of the jet on base pressure is indicated by the variations of base pressure coefficient $C_{p,b}$ and is presented in figure 9. For comparison purposes, base pressure coefficients of conventional nozzles are included on this figure. At comparable Mach numbers, although the general trend is the same, the jet did not increase the base pressure coefficient of the convergent-divergent plug-nozzle configuration as much as for a conventional convergent-divergent nozzle (fig. 9(a)). However, with the plug in the convergent position (fig. 9(b)) the effect of the jet on the base pressure coefficient was similar to that observed for a conventional convergent nozzle. It should be noted that the difference in flow angles and the jet expansion effect discussed previously in this section are factors influencing these curves.

Presented in figure 10 is the variation of the total external drag coefficient for both plug positions at free-stream Mach numbers of 0.6, 1.6, and 2.0. It is felt that, although the absolute value of the total external drag is not significant because of interference from the support struts, the trend with pressure ratio is significant. Because of instrumentation failure for this particular investigation, external-drag values from the strain-gage balance could not be obtained from the drag connection as anticipated. The total external drag was, however, obtained by adding the measured boattail pressure drag and the measured base drag to the sum of the nose pressure plus the friction drag. The sum of these latter forces was obtained from an unpublished investigation which utilized the same basic model as well as the same over-all body length. The sharp decrease in total drag of the convergent plug position with increasing nozzle pressure ratio as compared with the total drag of the convergent-divergent position is the cumulative effect of pressure ratio on boattail and base drags.

Internal Characteristics

Nozzle mass-flow coefficients (see appendix B) are presented in figure 11 for the convergent plug position at free-stream Mach numbers of 2.0, 1.6, 0.6, and 0.1 and angles of attack of zero and 8°. Although the amount of data was limited and the scatter pronounced, it appears that there was very little effect of nozzle pressure ratio, free-stream Mach number, and angle of attack. Moreover, the average value of flow coefficient, which was 0.988, was equivalent to that of a well-designed conventional nozzle. Values of flow coefficient were not obtained with the plug in the convergent-divergent position. However, flow coefficients of the same order of magnitude as for the convergent plug position might be anticipated.

The internal thrust characteristics, obtained from force measurements, are presented in figure 12 as the ratio of measured thrust to ideal thrust (see appendix B) for a range of free-stream Mach numbers and for angles of attack of zero and 8°. The variation of thrust ratio with nozzle pressure ratio for the convergent-divergent position of the plug is presented in figure 12(a). Within the data scatter, there appeared to have been very little effect of either free-stream Mach number or angle of attack on jet thrust. Contrary to expectations, the peak jet-thrust ratio, a value of 0.98, did not decrease for pressure ratios above the design value of 5.8 but held essentially constant.

For the convergent plug position (fig. 12(b)), there was generally little if any effect of free-stream Mach number or angle of attack on the jet thrust. The general level of the thrust ratio was low, a peak of 0.935 at P_3/p_0 of 4.0, and was probably caused by negative thrust being exerted on the protruding portion of the plug at the low pressure ratios. Moreover, in contrast with conventional convergent nozzles, only a small decrease in the thrust ratio was observed as the nozzle pressure ratio was increased above 4.0.

Static-pressure distributions on the plug for the convergent-divergent plug position and for the convergent plug position are presented in figures 13 and 14, respectively. Data are presented at zero angle of attack over a range of pressure ratios for all free-stream Mach numbers.

As indicated in figure 13, the flow for the convergent-divergent plug position generally expanded supersonically, and very good agreement was obtained with the isentropic one-dimensional flow theory. When the nozzle became far overexpanded ($P_3/p_0<2.8$), a shock entered the nozzle. For such operation, the internal shock system assumed a structure such that the static pressure at the nozzle exit was very close to ambient.

With the plug in the convergent position, the static-pressure distributions (fig. 14) indicate that the flow initially expanded very rapidly from the throat along the extended section of the plug. In fact, the initial expansion was so rapid that the flow appears to have expanded below ambient static pressure at all pressure ratios and all free-stream Mach numbers investigated. Generally, the flow exhibited the characteristics of expansion in a diverging-nozzle section.

Presented in figure 15 are typical schlieren photographs of the flow at the nozzle exit for the convergent plug position at three different pressure ratios for each of the Mach numbers of 2.0 and 0.6 and at zero angle of attack. These photographs serve to indicate the type of shock structure which produced the pressure distributions of figure 14.

Angle-of-attack data at 8° were obtained for the convergent plug position at Mach numbers of 2.0 and 1.6. Comparison of pressure distributions on the top and bottom of the plug indicated that up to an 8° angle of attack no asymmetric loads were applied to the plug.

An alternative method of obtaining jet thrust was employed in obtaining the nozzle thrust values given in figure 16. The change in jet thrust through the diverging-nozzle section was obtained from an integration of the static wall pressures in this section, and the result was added to the computed thrust of a sonic nozzle to obtain the resulting jet thrust at the exit. The jet thrust thus obtained neglected any friction losses in the nozzle. For purposes of comparison, the thrust-ratio curves obtained from the force measurements are included in this figure.

Up to a nozzle pressure ratio of 7.0, for the convergent-divergent plug position (fig. 16(a)), the thrust data obtained from the pressure distributions were approximately 2 percent above the same data obtained from force measurements. Above pressure ratios of 7.0, the two sets of data disagree in trend. The thrust ratio obtained from pressure integration peaked at the design point and then decreased as the nozzle became underexpanded. This trend is consistent with conventional convergent-divergent nozzle performance (ref. 7). On the other hand, the jet-thrust ratio determined from force measurements remained essentially constant as the nozzle was underexpanded. Generally the two sets of data agreed within 2 to 3 percent.

Agreement within 1 percent is indicated for the convergent plug position (fig. 16(b)). Only data above pressure ratios of 5.0 have been plotted since the instrumentation was found to be inadequate at lower pressure ratios because of the numerous shocks and the resulting abrupt pressure changes occurring on the plug below this pressure ratio. The pressure integration indicated that at low pressure ratios the protruding plug contributed a drag force. This drag force decreased in magnitude

as the nozzle pressure ratio was increased until the extended section of the plug contributed a thrust force in the high-pressure-ratio range. This variation in force on the protruding plug no doubt caused the thrust-ratio curve to exhibit the flat characteristics shown.

Compared in figure 17(a) are the thrust ratios for three convergent-divergent nozzles. A comparison of the data obtained in the present investigation with data obtained on a similar plug nozzle investigated in quiescent air (ref. 3) indicates excellent agreement. It also appears that the convergent-divergent plug-type nozzle was comparable on a thrust-ratio basis with a conventional-type nozzle (ref. 7) having essentially the same design point.

A comparison of convergent-type nozzles is made in figure 17(b). Good agreement was again obtained between the present investigation and an investigation on a comparable plug-type nozzle in quiescent air (ref. 4). As expected, the thrust ratio for the plug nozzle was below that of a conventional convergent nozzle (ref. 7) in the low-pressure-ratio range and compared more favorably as the pressure ratio was increased.

Jet-Thrust-Minus-Drag Comparison

A comparison is made in figure 18 of the jet-thrust-minus-drag characteristics of the plug nozzle and comparable conventional nozzles. Calculations were made for the basic model used in the present investigation having a nozzle throat area of 0.090 square foot. The performance of the conventional nozzles was estimated from the thrust data of reference 7 and unpublished drag data such as is shown in figures 7 and 9. It should be noted that the inlet momentum for an over-all engine application was not included in figure 18, thus the use of jet thrust rather than net thrust.

The jet-thrust-minus-drag performance of the plug nozzle with the convergent-divergent position (fig. 18(a)) was comparable over the entire range with that of a conventional convergent-divergent nozzle having essentially the same design point. With the plug in the convergent position (fig. 18(b)), the thrust-minus-drag performance of the plug nozzle also compared favorably over the entire range with a conventional convergent nozzle. The low thrust ratios noted for this plug position in the low-pressure-ratio region (fig. 17(b)) were evidently more than compensated for by the smaller amount of boattail drag (fig. 7(b)).

SUMMARY OF RESULTS

The following results were obtained from an investigation conducted in the 8- by 6-foot supersonic wind tunnel on a plug-type exhaust nozzle tested in a convergent and a convergent-divergent position with an expansion ratio of 1.45:

1. The thrust-minus-drag performance of the plug nozzles investigated compared favorably over the entire pressure-ratio range with conventional nozzles having the same design points.

2. Internal performance was generally insensitive to external flow and was essentially the same for the range of free-stream Mach numbers investigated as obtained on comparable plug nozzles investigated in quiescent air.

3. The effect of the exhaust jet on the external aerodynamics was similar to that for conventional nozzles in that the boattail drag and the base pressure were more influenced by the convergent position than by the convergent-divergent position.

4. Nozzle flow coefficients with choked flow of the same order of magnitude as for conventional nozzles were virtually unaffected by pressure ratio and external flow.

5. During angle-of-attack operation, no asymmetric loads were obtained on the plug when extended beyond the afterbody.

Lewis Flight Propulsion Laboratory
National Advisory Committee for Aeronautics
Cleveland, Ohio, December 11, 1953

APPENDIX A

SYMBOLS

The following symbols are used in this report:

A	area, sq ft
B_D	strain-gage-balance reading for drag connection, lb
B_{F-D}	strain-gage-balance reading for thrust-minus-drag connection, lb
C_D	drag coefficient, D/q_0A_m
$C_{F,c}$	corrected thrust coefficient, F_c/q_0A_m
C_f	flow coefficient, m/m_i
C_p	pressure coefficient, $(p - p_0)/q_0$
D	drag force, lb
F	jet thrust, $mV_4 + A_4(p_4 - p_0)$, lb
F_c	jet thrust based on throat area of 0.090 sq ft, lb
F_i	ideal jet thrust, $mV_{4,i}$, lb
F/F_i	thrust ratio
f/a	fuel-air ratio
g	acceleration due to gravity, 32.2 ft/sec^2
J	total momentum, $mV + Ap$, lb
M	Mach number
m	mass flow, ρAV, slug/sec
P	total pressure, lb/sq ft
P_3/p_0	nozzle pressure ratio
p	static pressure, lb/sq ft
q	dynamic pressure, $\gamma pM^2/2$, lb/sq ft

R	radius, ft
T	total temperature, $^{\circ}R$
V	velocity, ft/sec
γ	ratio of specific heats for air
ρ	static density, slug/cu ft

Subscripts:

a	boattail
b	base
i	ideal
m	maximum
t	total
0	free stream
1	before shoulder
2	after shoulder
3	nozzle entrance
4	nozzle exit
*	nozzle throat

APPENDIX B

DATA REDUCTION

External Drag

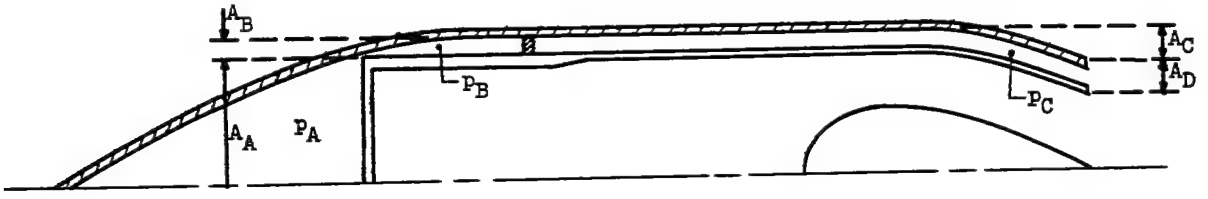

Sketch 1

Total external drag was obtained from the model by use of the drag connection of the strain-gage balance and various pressure measurements. In sketch 1,

$$D_t = B_D + (p_A - p_O)A_A + (p_B - p_O)A_B - (p_C - p_O)A_C - (p_C - p_O)A_D \quad (B1)$$

Measured Jet Thrust

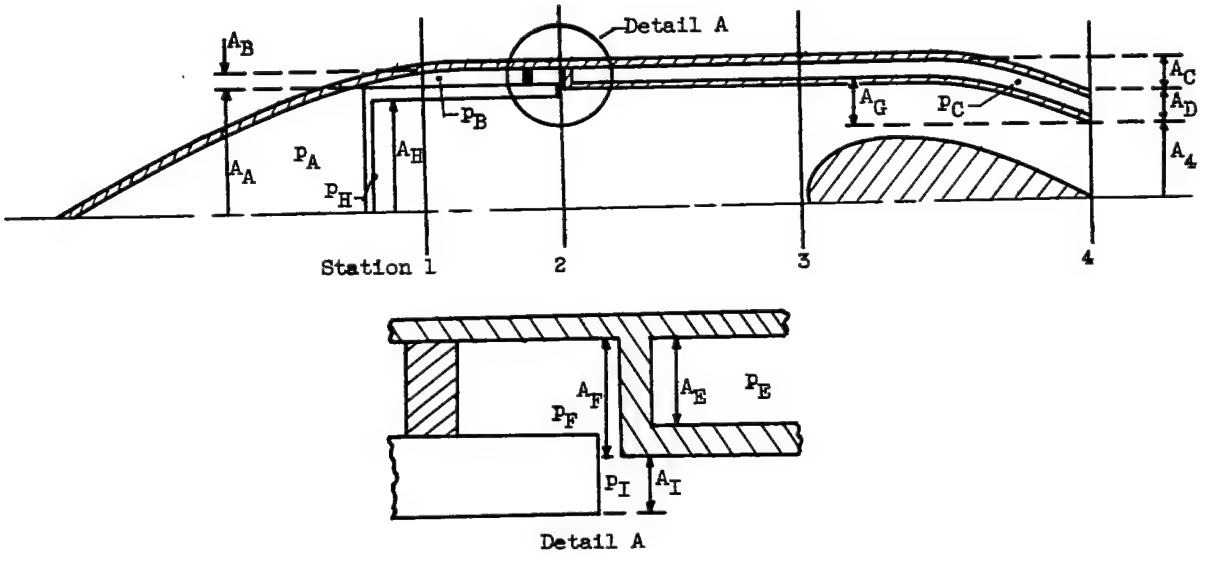

Sketch 2

Jet thrust is defined as

$$F_4 = mV_4 + p_4A_4 - p_0A_4 \tag{B2}$$

Equation (B2) is equivalent to

$$F_4 = J_4 - p_0A_4 \tag{B3}$$

The momentum at station 4 is related to the momentum at station 2 by

$$J_4 = J_2 - \Delta J_{2-3} - \Delta J_{3-4} \tag{B4}$$

Calibration indicated that ΔJ_{2-3} was equal to zero, and since

$$J_2 = p_HA_H + p_IA_I$$

equation (B3) becomes

$$F_4 = p_HA_H + p_IA_I - \Delta J_{3-4} - p_0A_4 \tag{B5}$$

The change in total momentum between stations 3 and 4 is equal to the absolute force acting on the nozzle (i.e., the inner liner and plug between these two stations). This force plus the total external drag is obtained from the thrust-minus-drag connection of the strain-gage balance:

$$\Delta J_{3-4} + D_t = B_{F-D} + (p_A - p_0)A_A + (p_B - p_0)A_B - (p_C - p_0)A_C - (p_C - p_0)A_D + p_CA_G + p_EA_E - p_FA_F \tag{B6}$$

Substitution of ΔJ_{3-4} from equation (B6) into equation (B5) yields the jet thrust minus the total external drag of the model:

$$F_4 - D_t = p_HA_H + p_IA_I - B_{F-D} - (p_A - p_0)A_A - (p_B - p_0)A_B + (p_C - p_0)A_C + (p_C - p_0)A_D - p_CA_G - p_EA_E + p_FA_F - p_0A_4 \tag{B7}$$

The jet thrust can then be calculated by adding a total-external-drag value to the value of jet-thrust-minus-external-drag as obtained from equation (B7).

Ideal Jet Thrust

Ideal jet thrust is defined as the product of the measured mass flow and the ideal exit velocity for complete isentropic expansion.

(A truly ideal nozzle would have the same thrust but with a throat area slightly smaller by the amount of the mass-flow coefficient.) Thus,

$$F_i = mV_{4,i} \tag{B8}$$

Equation (B8) is equivalent to

$$F_i = m\left[\left(\frac{2\gamma gRT_1}{\gamma - 1}\right)\frac{\left(\frac{P_3}{P_0}\right)^{\frac{\gamma-1}{\gamma}} - 1}{\left(\frac{P_3}{P_0}\right)^{\frac{\gamma-1}{\gamma}}}\right]^{1/2} \tag{B9}$$

The total temperature T_1 of the internal air flow was measured by thermocouples located in the horizontal support struts and was assumed to remain constant throughout the model.

Nozzle Mass-Flow Coefficient

The mass-flow coefficient is defined as the ratio of mass flow actually passed through the nozzle to the amount of mass flow that can ideally be passed through the nozzle. Thus,

$$C_f = \frac{m(1 + f/a)}{P_3 A_* \left(\frac{2}{\gamma + 1}\right)^{\frac{\gamma+1}{2(\gamma-1)}} \sqrt{\frac{\gamma}{gRT_1}}}$$

REFERENCES

1. Lundin, Bruce: Investigation of Several Clamshell Variable-Area Exhaust Nozzles for Turbojet Engines. NACA RM E9B02, 1949.

2. Fleming, William A.: Internal Performance of Several Types of Jet-Exit Configurations for Supersonic Turbojet Aircraft. NACA RM E52K04, 1953.

3. Krull, H. George, Steffen, Fred W., and Ciepluch, Carl C.: Internal Performance Characteristics of Variable-Throat Plug- and Vaned-Type Convergent-Divergent Nozzles. NACA RM E53D09, 1953.

4. Ciepluch, Carl C., Krull, H. George, and Steffen, Fred W.: Preliminary Investigation of Performance of Variable-Throat Extended-Plug-Type Nozzle over Wide Range of Nozzle Pressure Ratios. NACA RM E53J28, 1954.

5. Sterbentz, William H., and Wilcox, Fred A.: Investigation of Effects of Movable Exhaust-Nozzle Plug on Operational Performance of 20-Inch Ram Jet. NACA RM E8D22, 1948.

6. Cortright, Edgar, and Kochendorfer, Fred D.: Jet Effects on Flow over Afterbodies in Supersonic Stream. NACA RM E53H25, 1953.

7. Krull, H. George, and Steffen, Fred W.: Performance Characteristics of One Convergent and Three Convergent-Divergent Nozzles. NACA RM E52H12, 1952.

TABLE I. - PRINCIPLE DIMENSIONS OF PLUG NOZZLE

[Minimum flow area for convergent-divergent plug position, 0.140 sq ft; minimum flow area for convergent plug position, 0.090 sq ft; expansion ratio of convergent-divergent plug position, 1.451; maximum model cross-sectional area, 0.371 sq ft.]

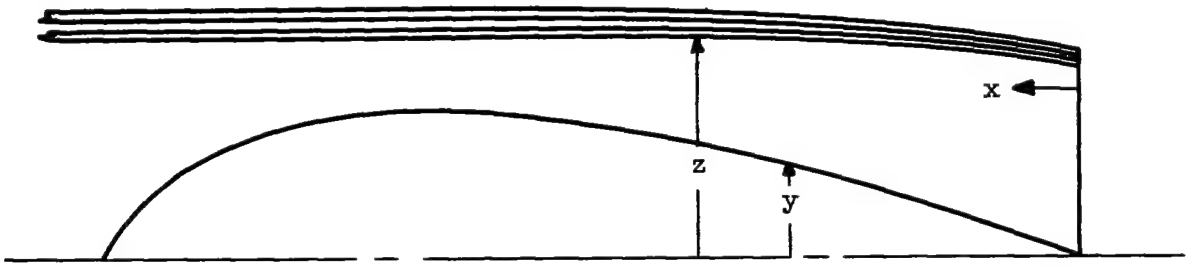

Coordinates of plug and nozzle		
x, in.	y, in.	z, in.
0	0	3.055
1.36	.631	3.170
1.93	.881	3.230
2.39	1.071	3.270
2.78	1.229	3.310
3.13	1.353	3.330
4.60	1.817	3.440
5.78	2.100	3.480
6.89	2.280	3.500
7.90	2.370	3.500
8.84	2.405	3.500
9.68	2.385	3.500
10.50	2.310	3.500
11.20	2.190	3.500
11.83	2.030	3.500
12.42	1.852	3.500
12.93	1.640	3.500
13.38	1.402	3.500
13.73	1.142	3.500
14.02	.872	3.500
14.21	.588	3.500
14.40	0	3.500

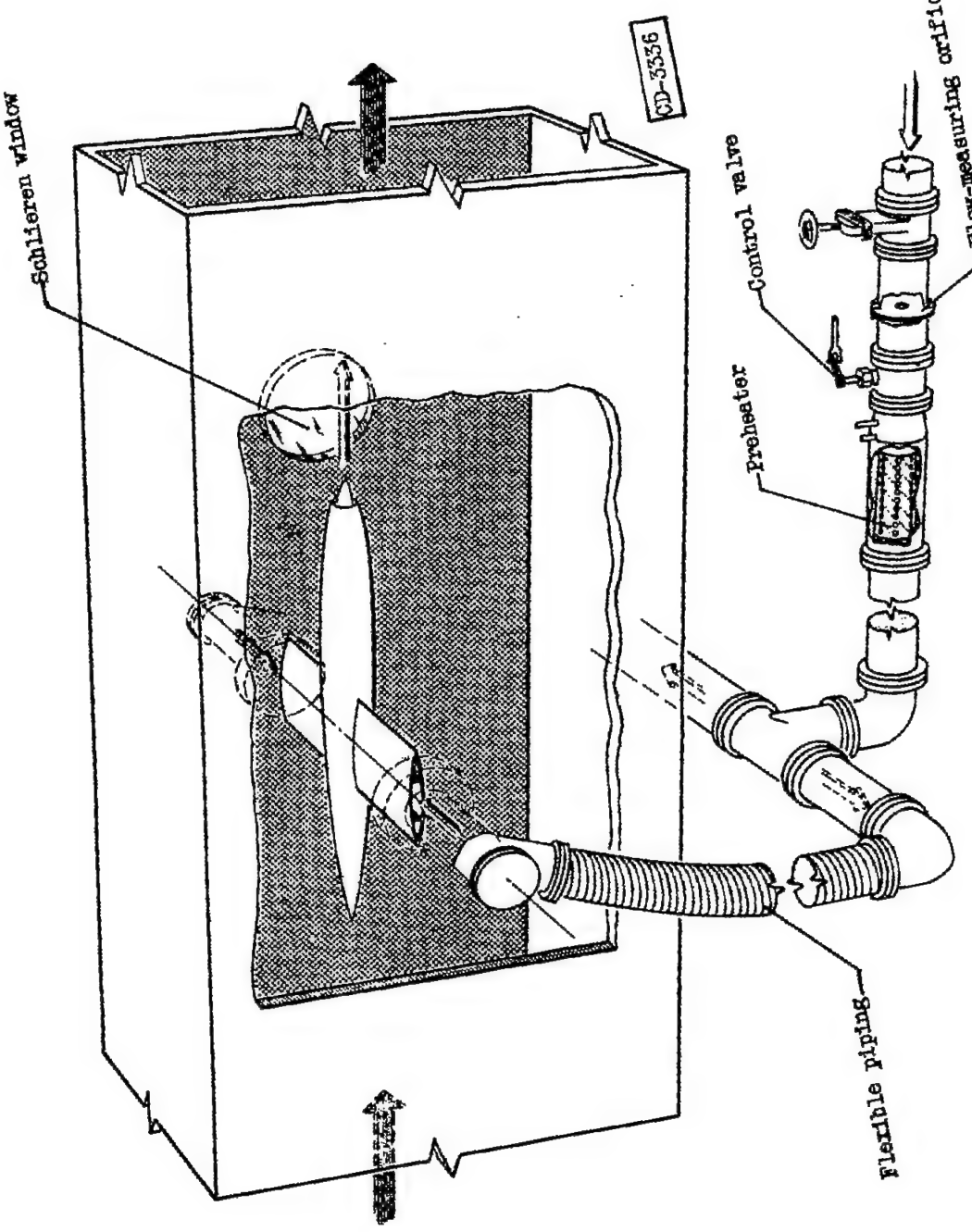

Figure 1. - Schematic drawing of jet-exit model installed in 8- by 6-foot supersonic wind tunnel.

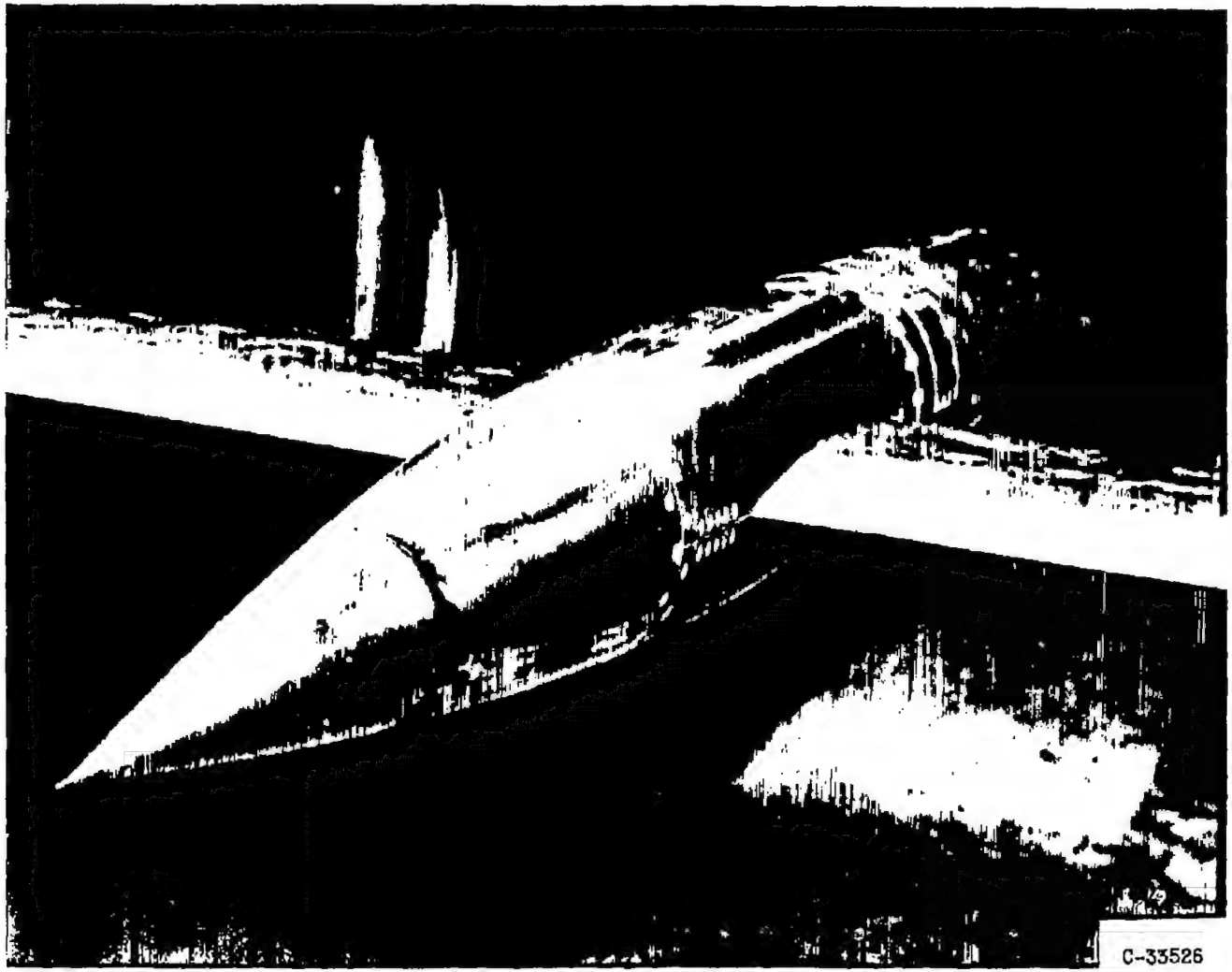

Figure 2. - Photograph of jet-exit model in 8- by 6-foot supersonic wind tunnel.

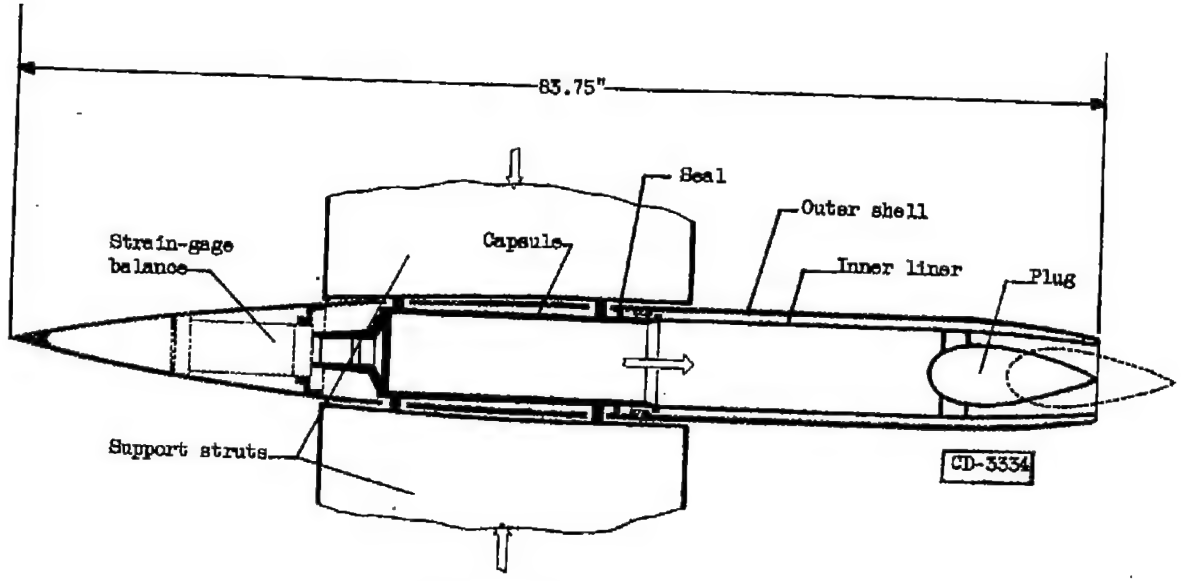

(a) "Drag" connection.

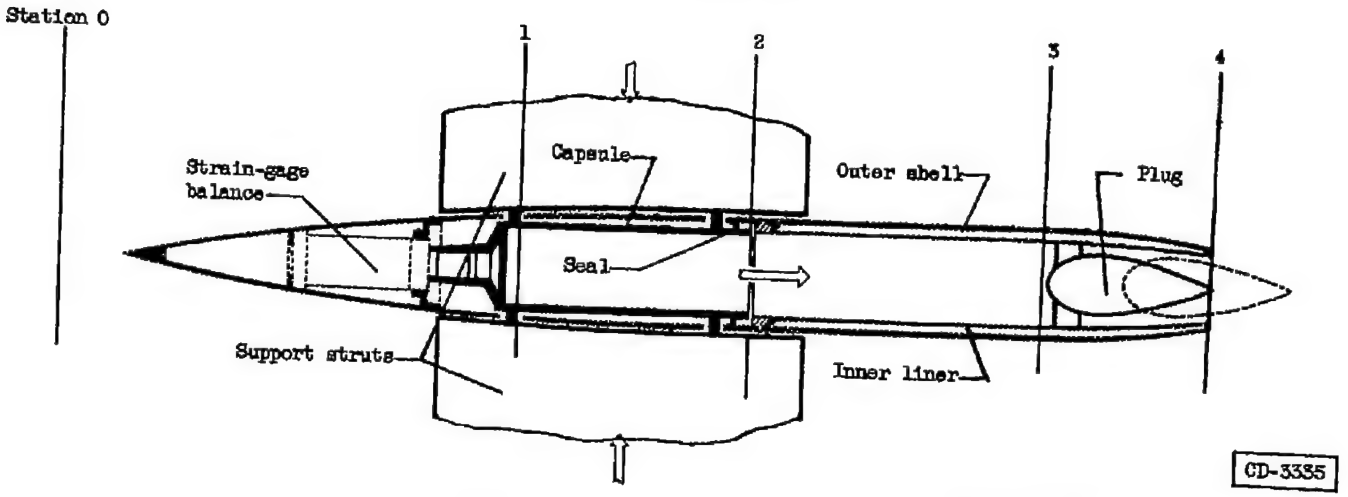

(b) "Thrust-minus-drag" connection.

Figure 3. - Schematic diagram of jet-exit model.

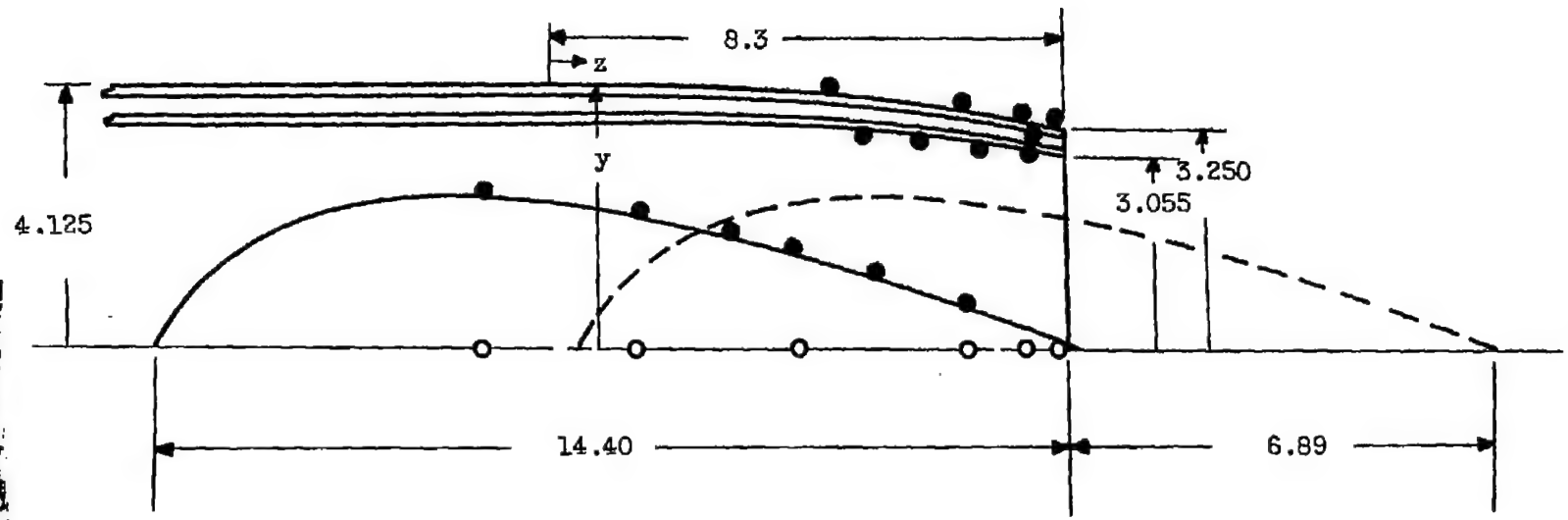

Equation of boattail: $y = 4\frac{1}{8}\left[1 - \left(\frac{z}{18}\right)^2\right]$

Static-pressure orifice

● Top and bottom

○ Side

Figure 4. - Schematic drawing of plug-nozzle - afterbody configuration including static-pressure instrumentation. (All dimensions in inches.)

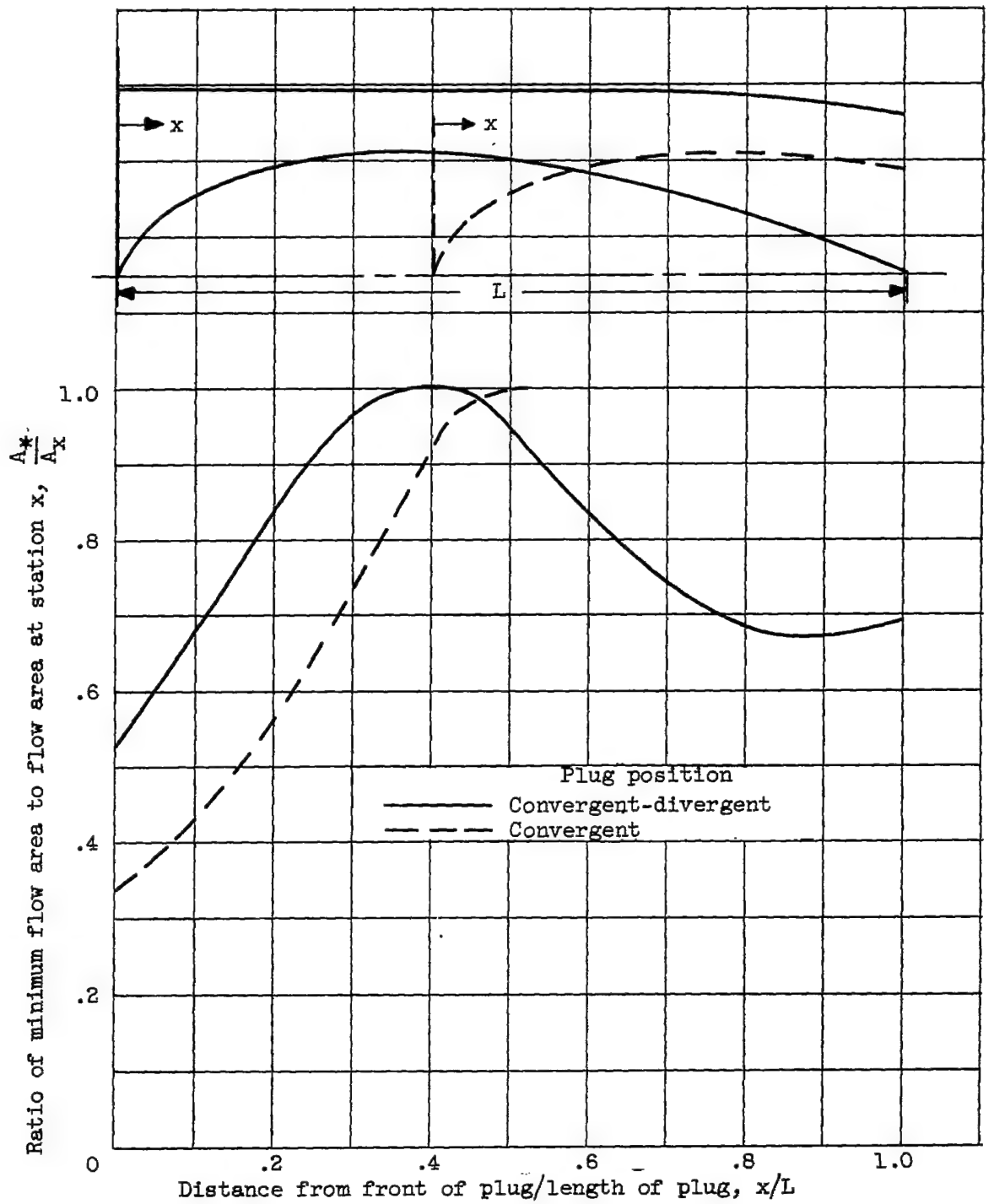

Figure 5. - Flow-area variation for two plug positions investigated.

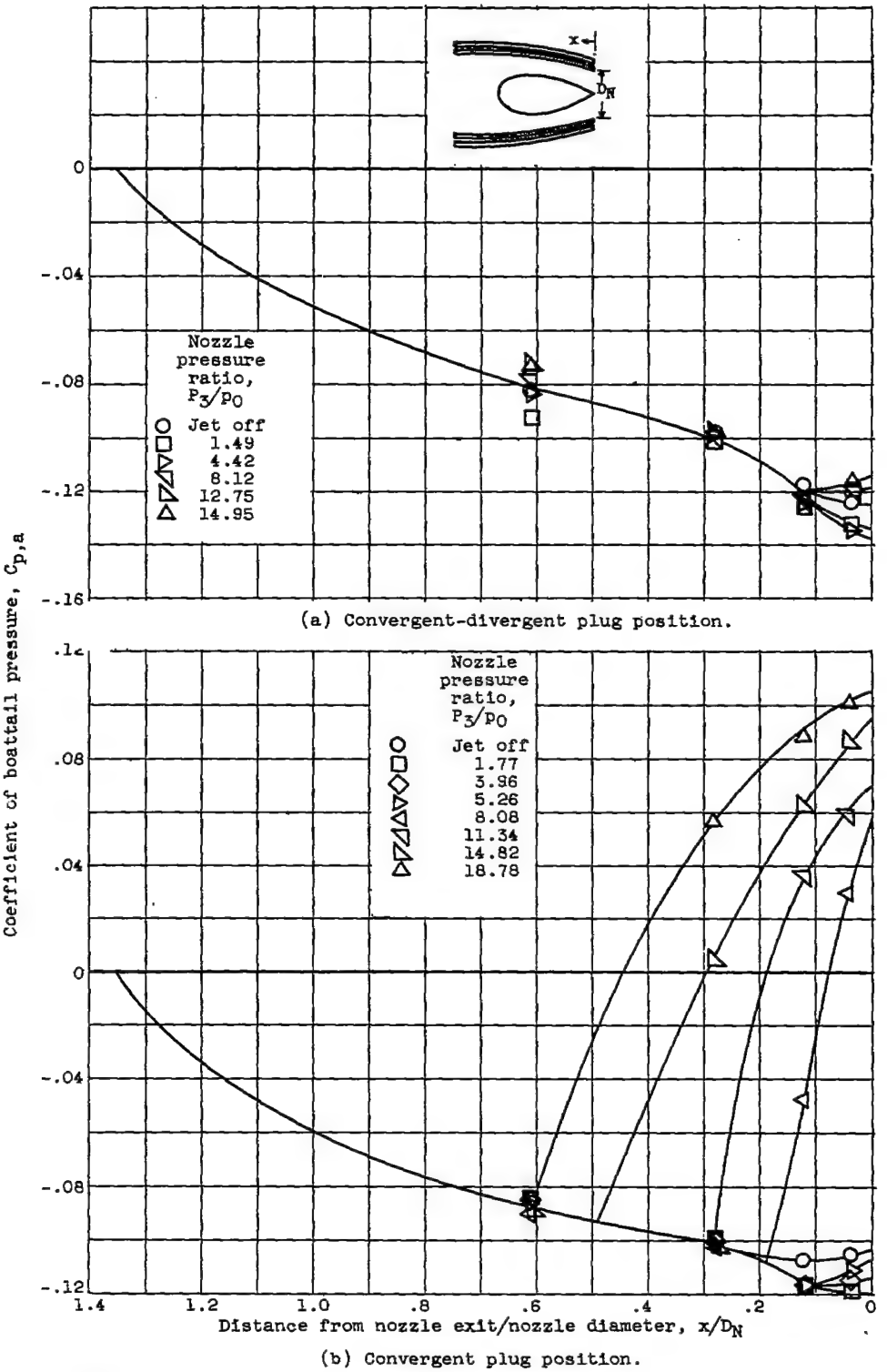

(a) Convergent-divergent plug position.

(b) Convergent plug position.

Figure 6. - Boattail pressure distributions at free-stream Mach number of 2.0 and zero angle of attack.

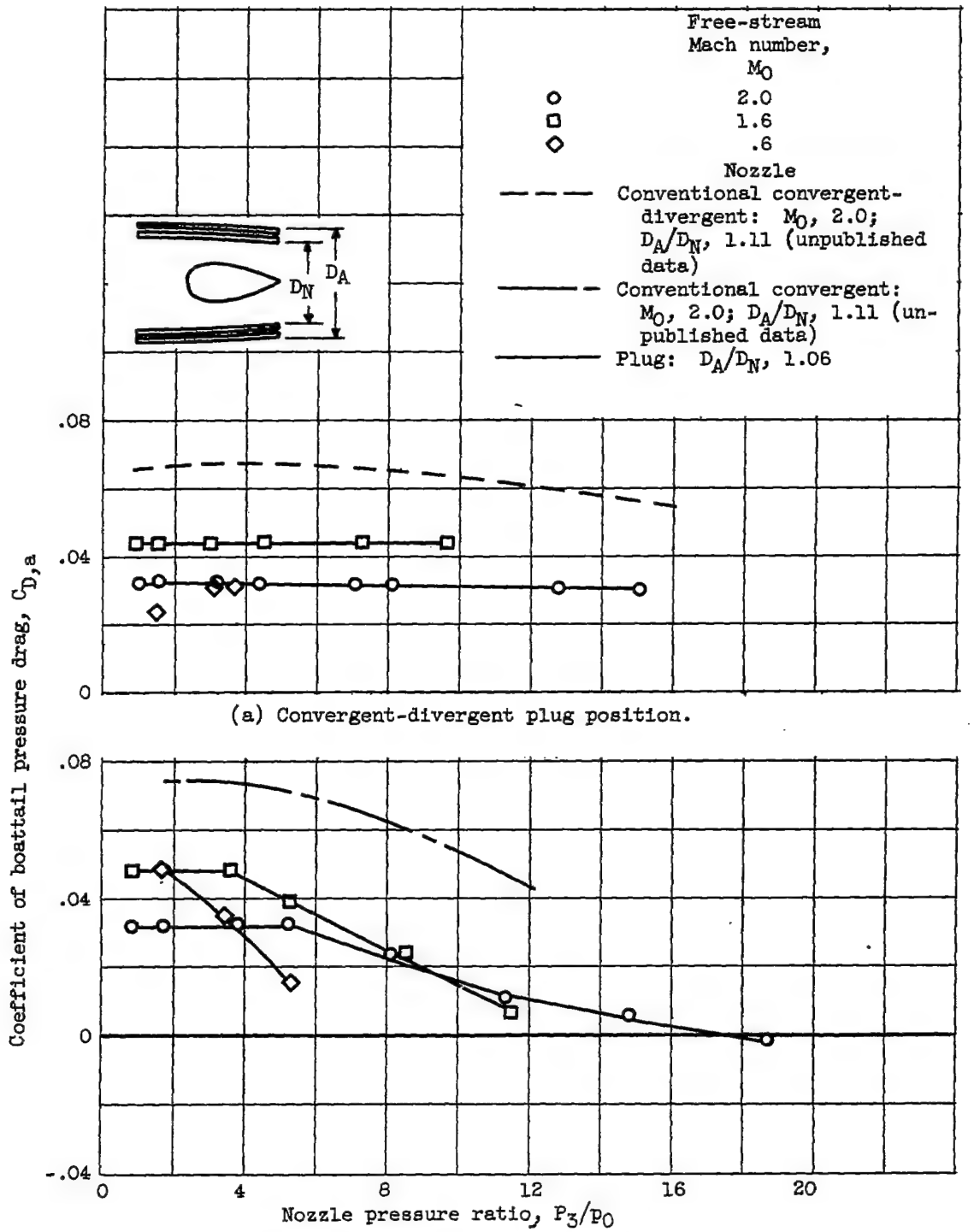

Figure 7. - Variation of boattail pressure-drag coefficient with nozzle pressure ratio at zero angle of attack.

[redacted]

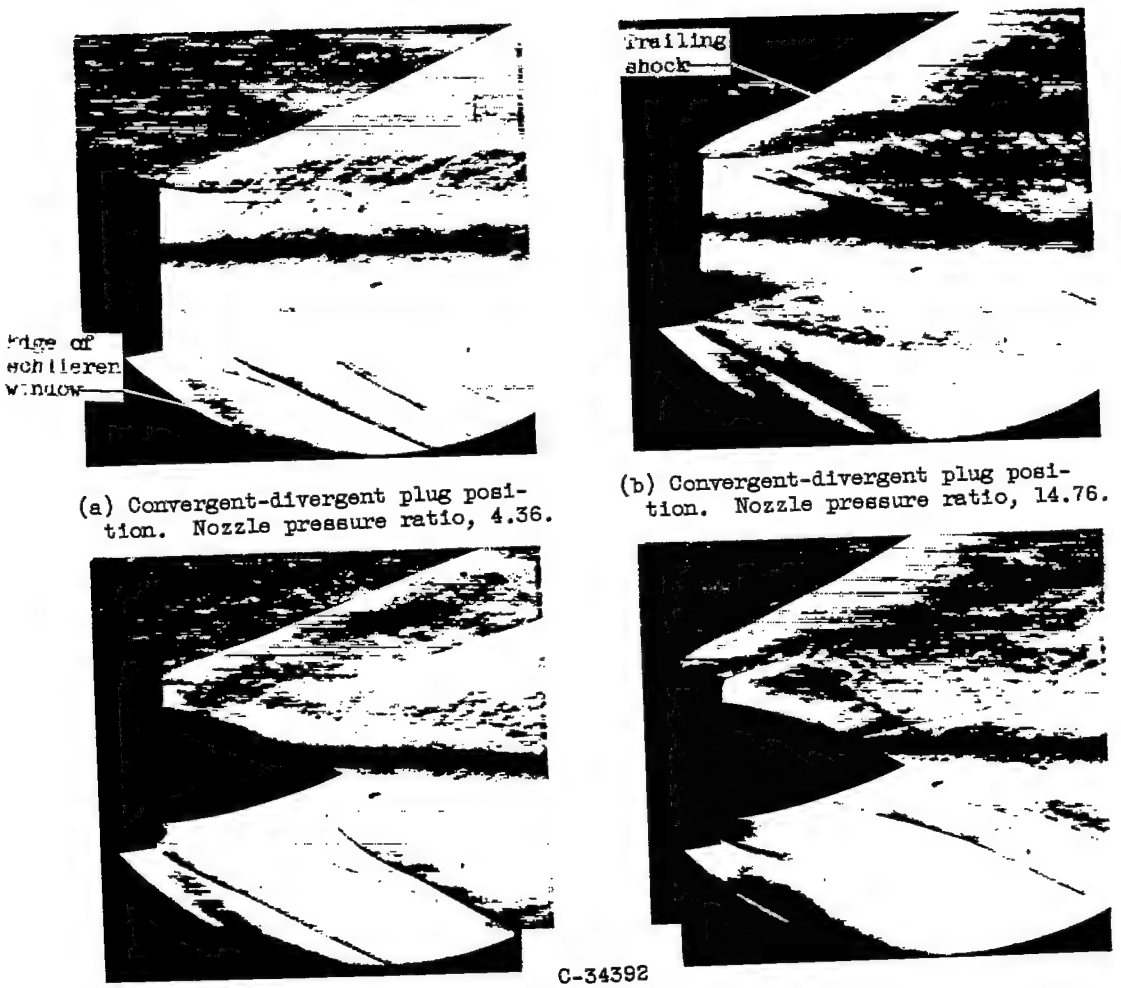

(a) Convergent-divergent plug position. Nozzle pressure ratio, 4.36.

(b) Convergent-divergent plug position. Nozzle pressure ratio, 14.76.

(c) Convergent plug position. Nozzle pressure ratio, 3.51.

(d) Convergent plug position. Nozzle pressure ratio, 14.26.

Figure 8. - Schlieren photographs of external aerodynamics of boattail at free-stream Mach number of 2.0 and zero angle of attack.

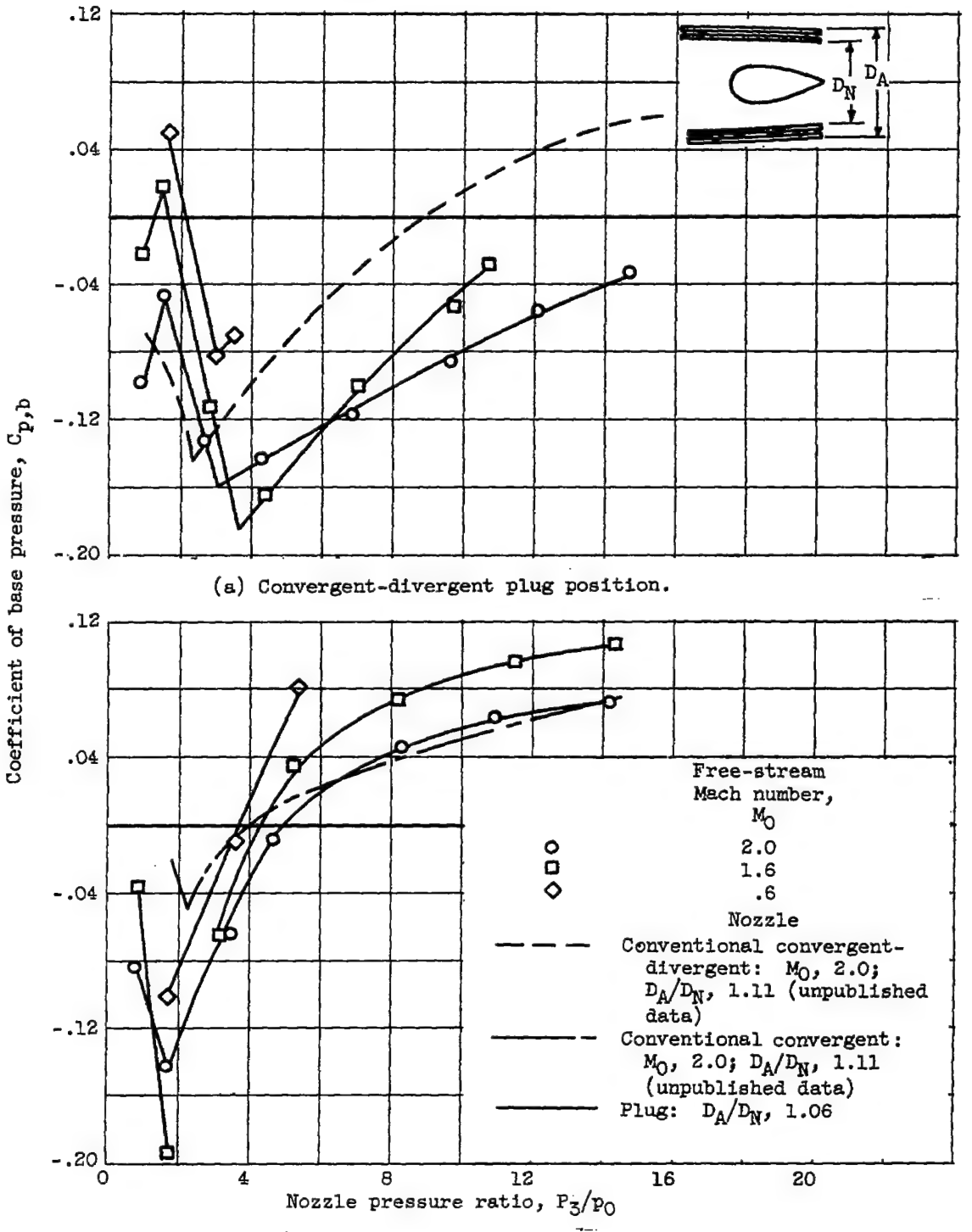

Figure 9. - Variation of base pressure coefficient with nozzle pressure ratio at zero angle of attack.

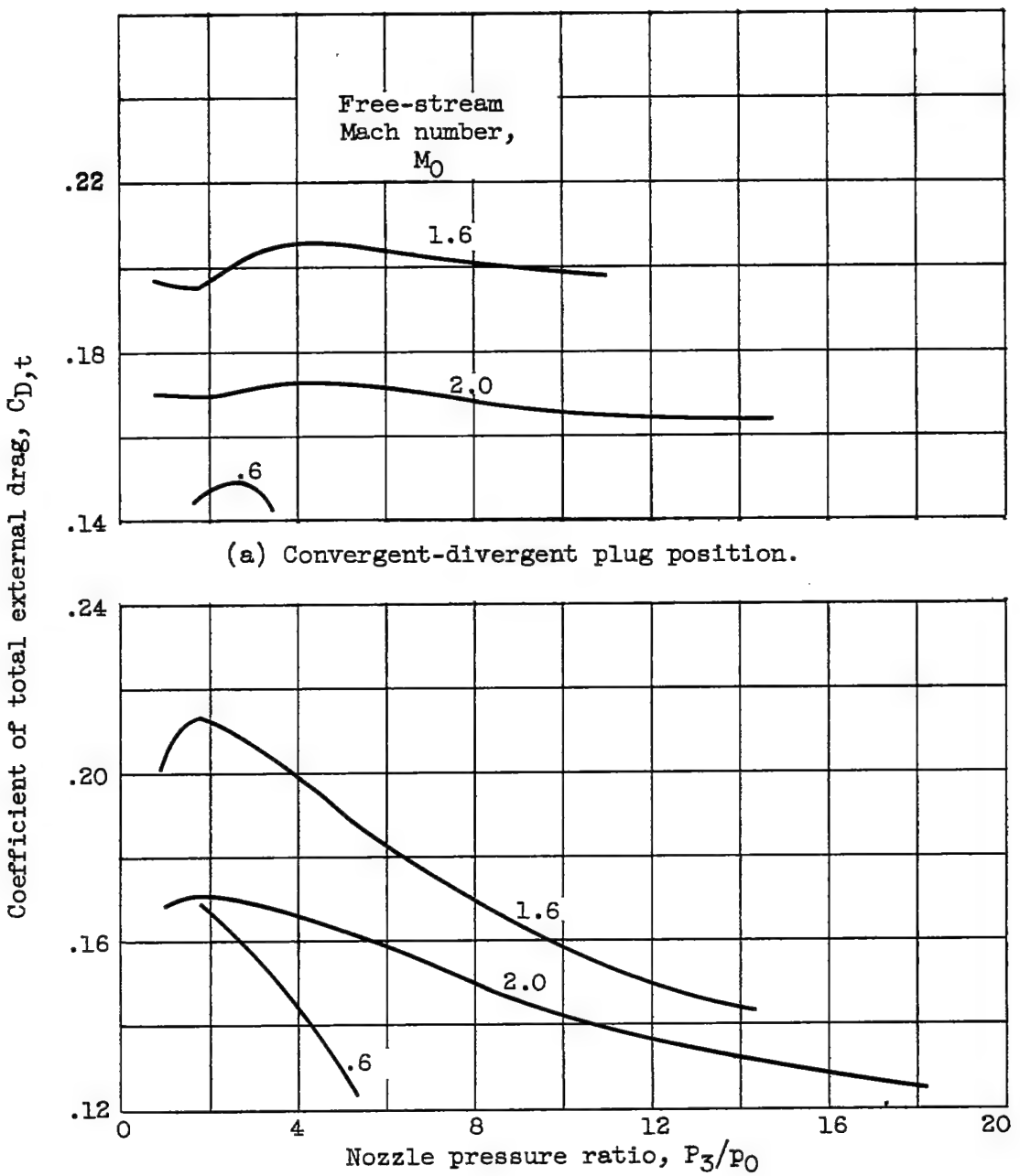

Figure 10. - Variation of total external drag coefficient with nozzle pressure ratio at zero angle of attack.

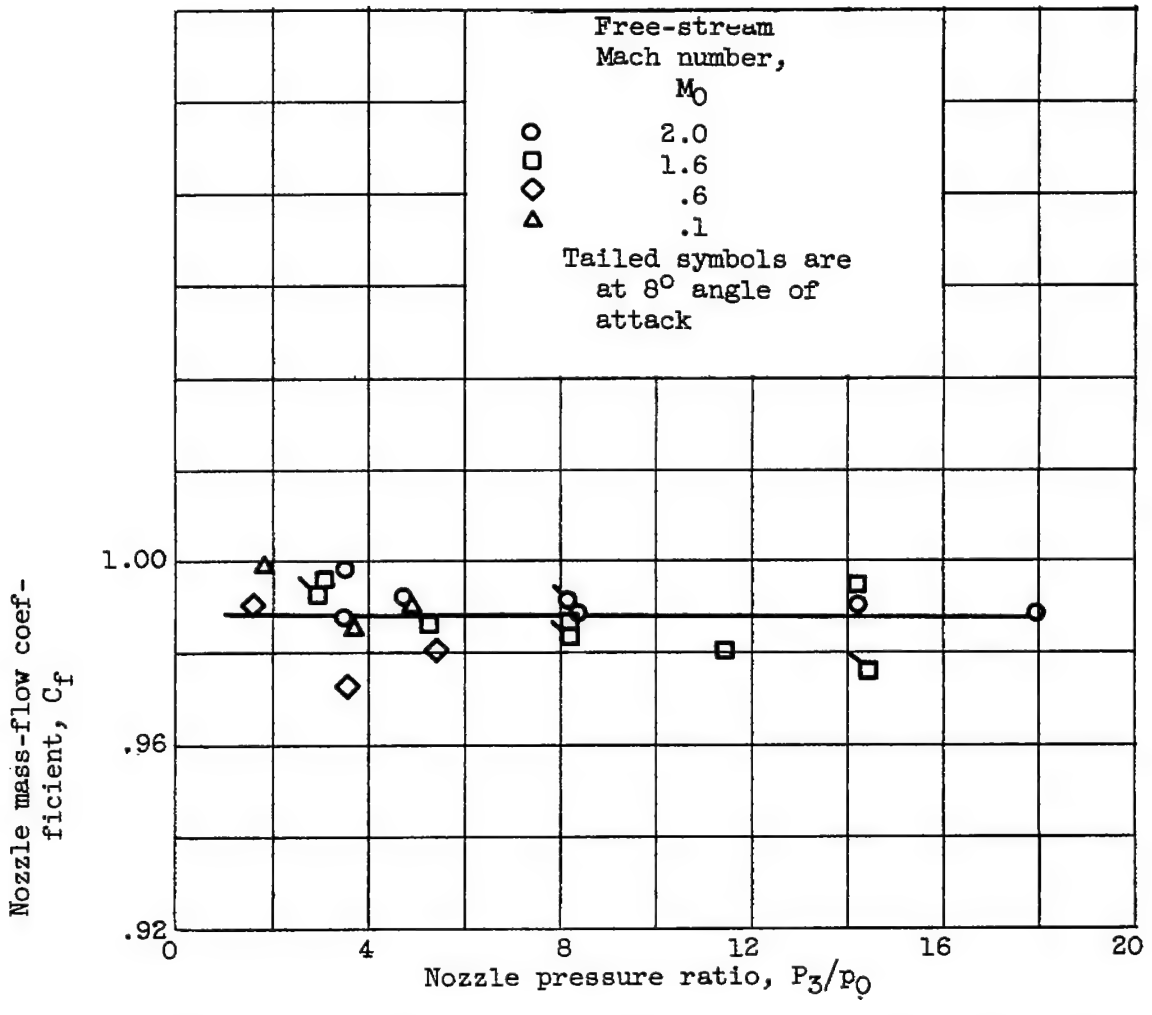

Figure 11. - Variation of nozzle mass-flow coefficient with nozzle pressure ratio for convergent plug position at zero angle of attack.

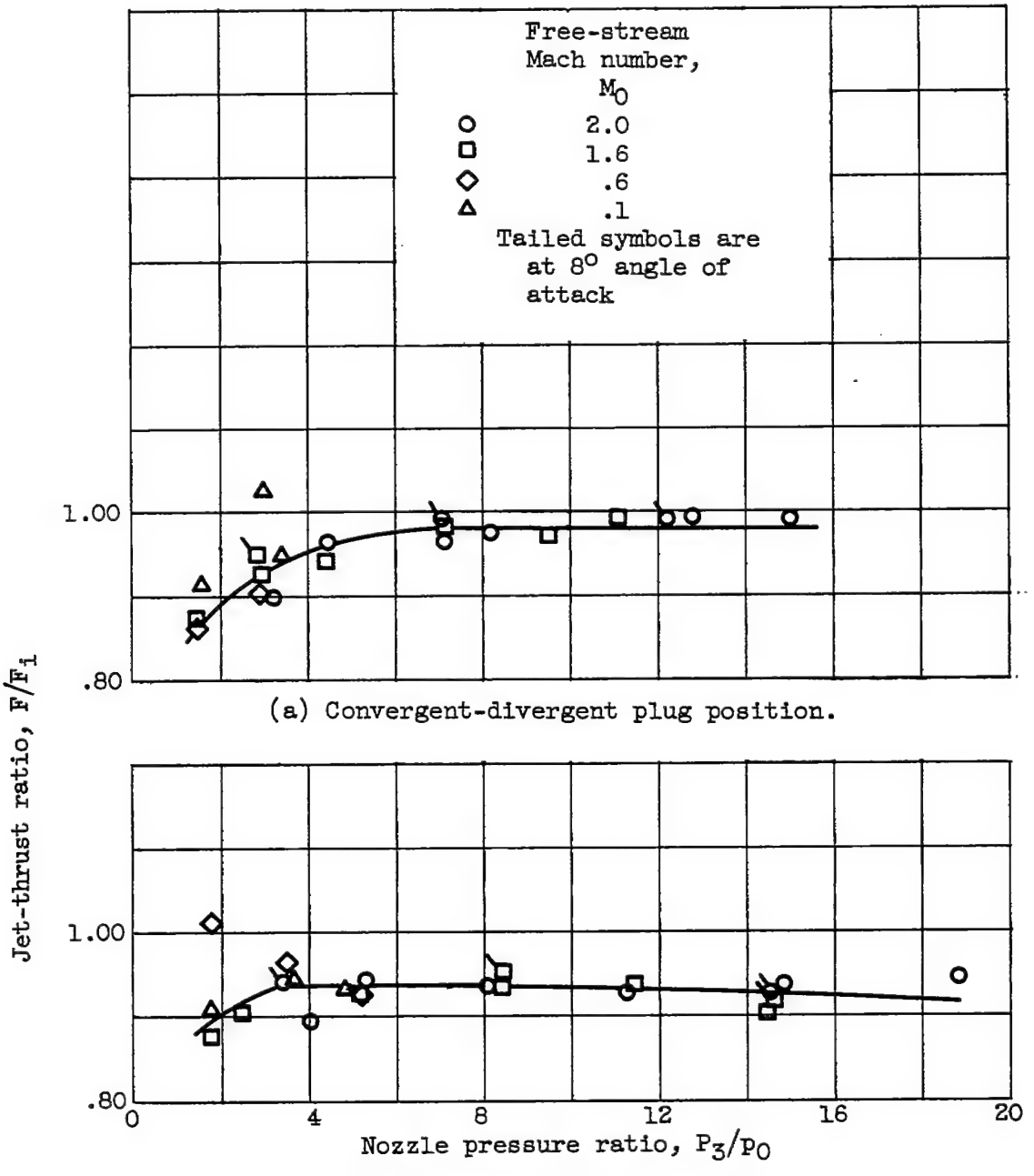

(a) Convergent-divergent plug position.

(b) Convergent plug position.

Figure 12. - Variation of jet-thrust ratio obtained from force measurements with nozzle pressure ratio at zero angle of attack.

[redacted]

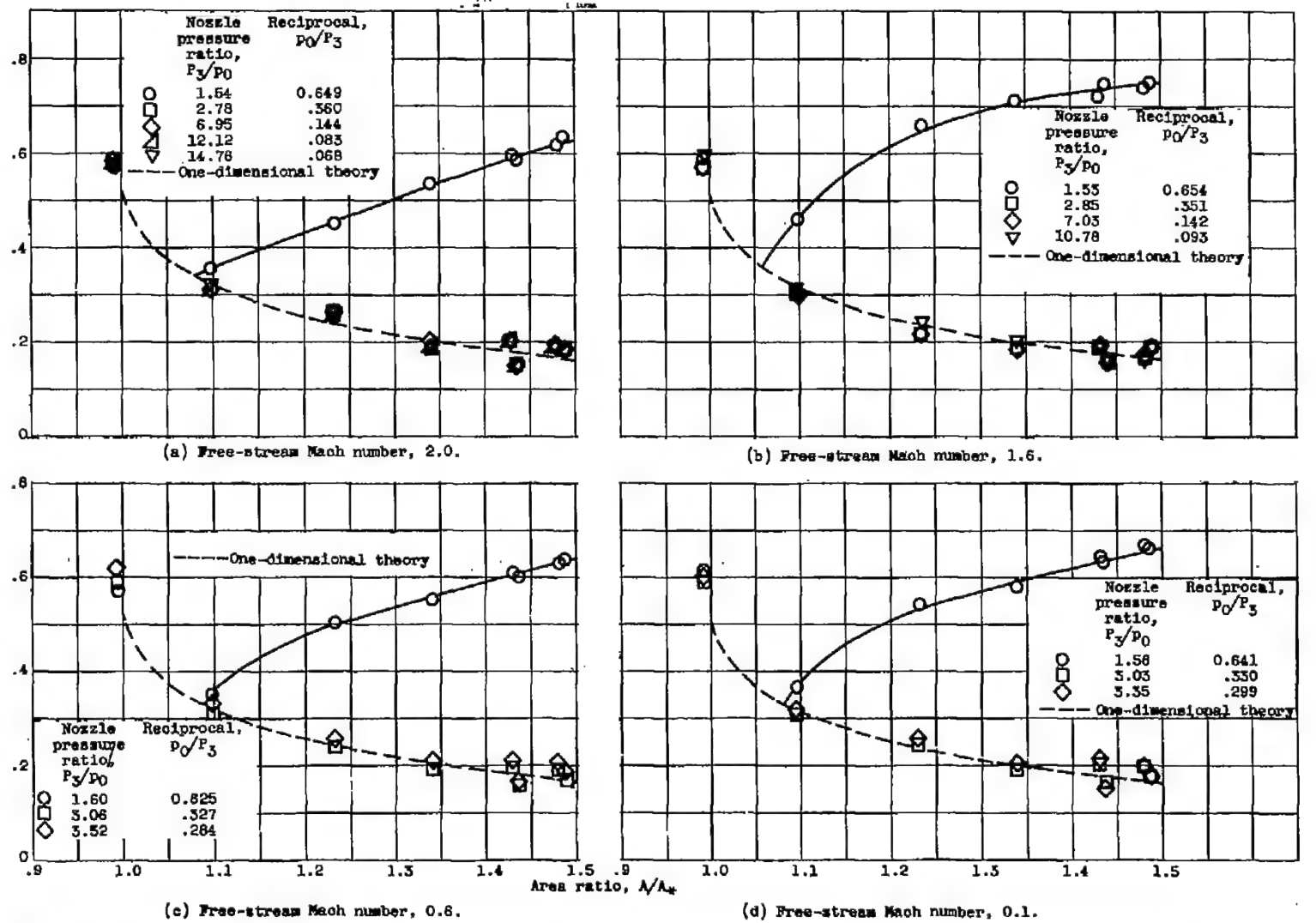

(a) Free-stream Mach number, 2.0.

(b) Free-stream Mach number, 1.6.

(c) Free-stream Mach number, 0.6.

(d) Free-stream Mach number, 0.1.

Figure 15. - Static-pressure distribution through diverging section for convergent-divergent plug position at zero angle of attack.

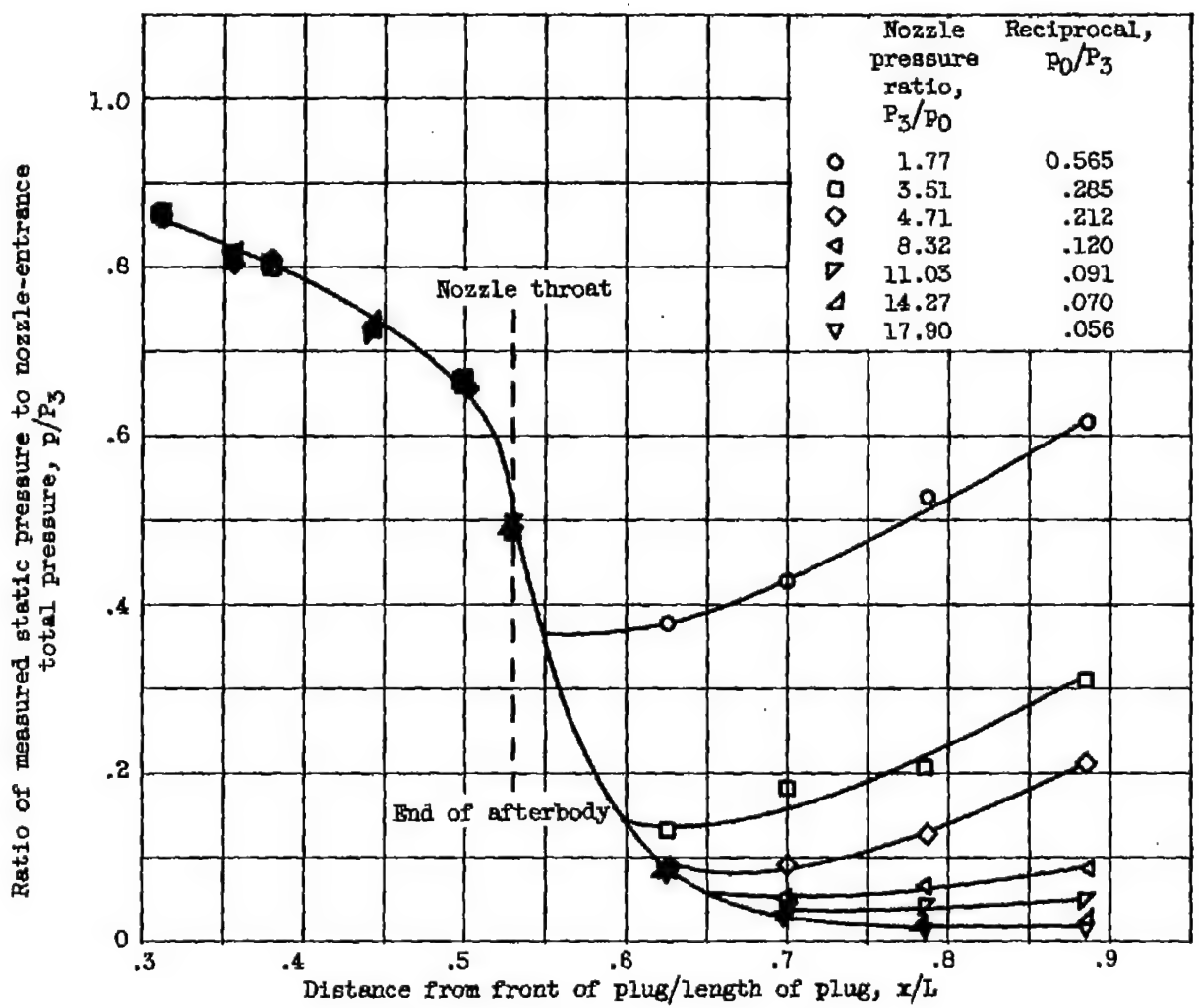

(a) Free-stream Mach number, 2.0.

Figure 14. - Static-pressure distributions along center plug for convergent plug position at zero angle of attack.

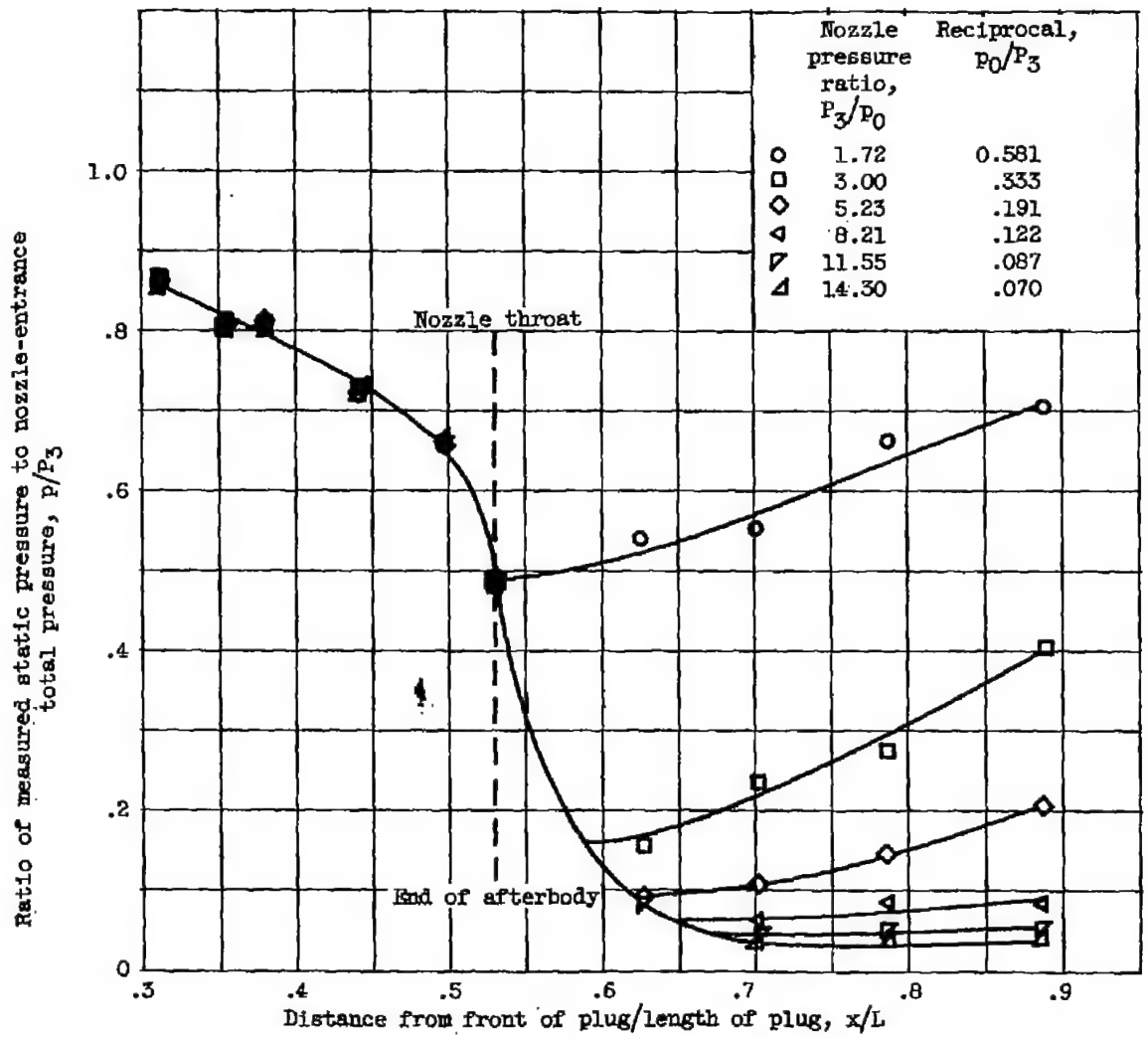

(b) Free-stream Mach number, 1.6.

Figure 14. - Continued. Static-pressure distributions along center plug for convergent plug position at zero angle of attack.

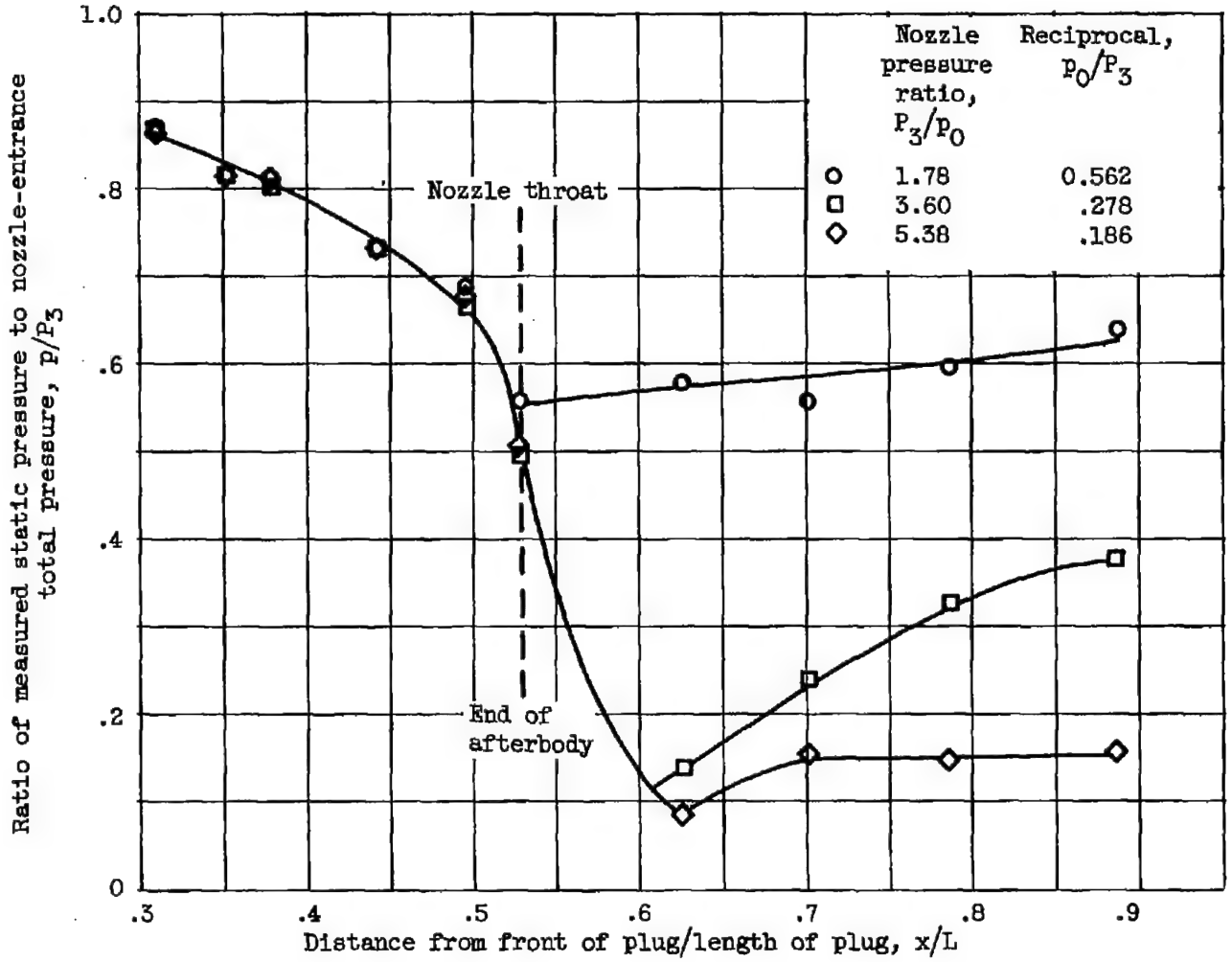

(c) Free-stream Mach number, 0.6.

Figure 14. - Continued. Static-pressure distributions along center plug for convergent plug position at zero angle of attack.

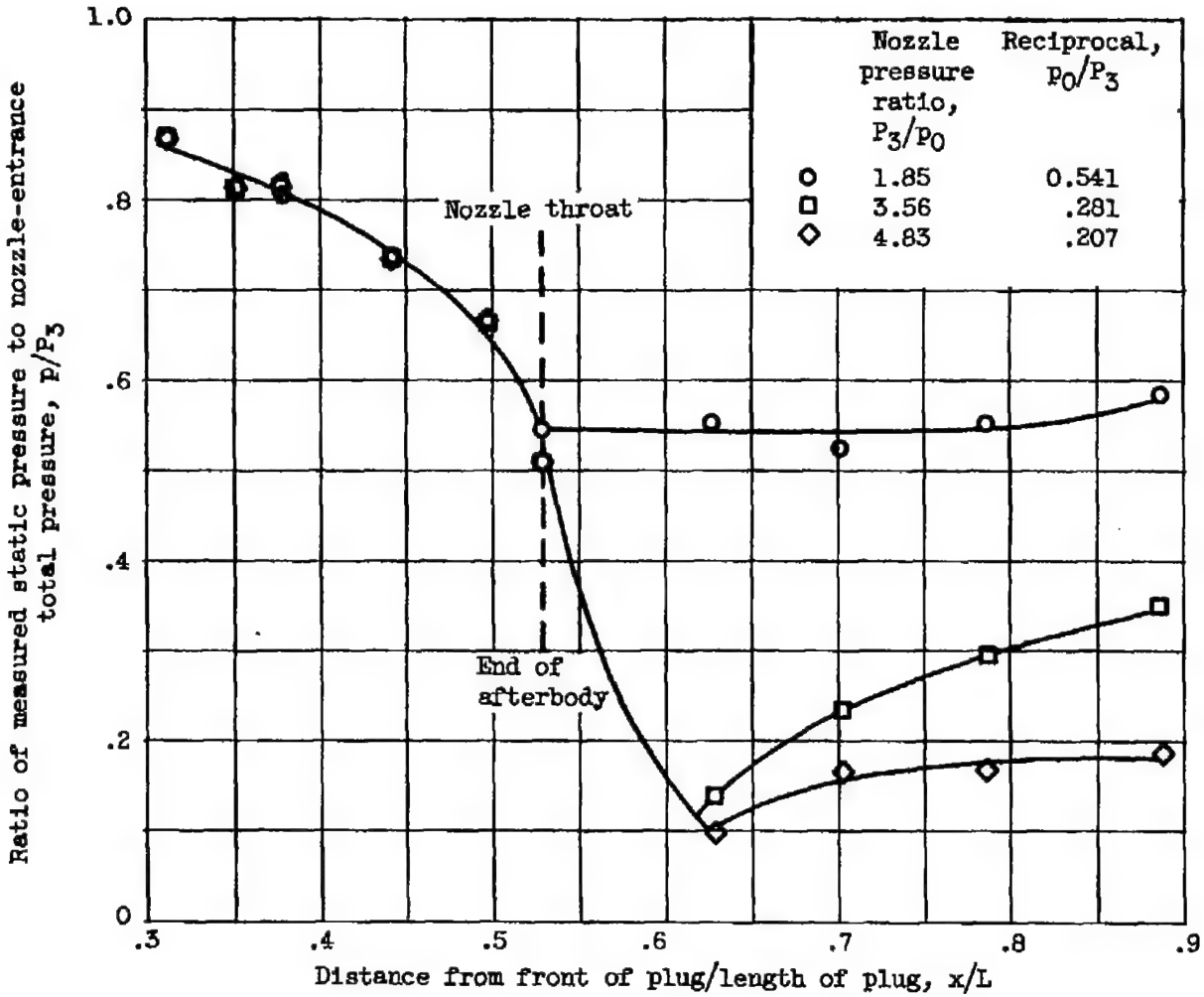

(d) Free-stream Mach number, 0.1.

Figure 14. - Concluded. Static-pressure distributions along center plug for convergent plug position at zero angle of attack.

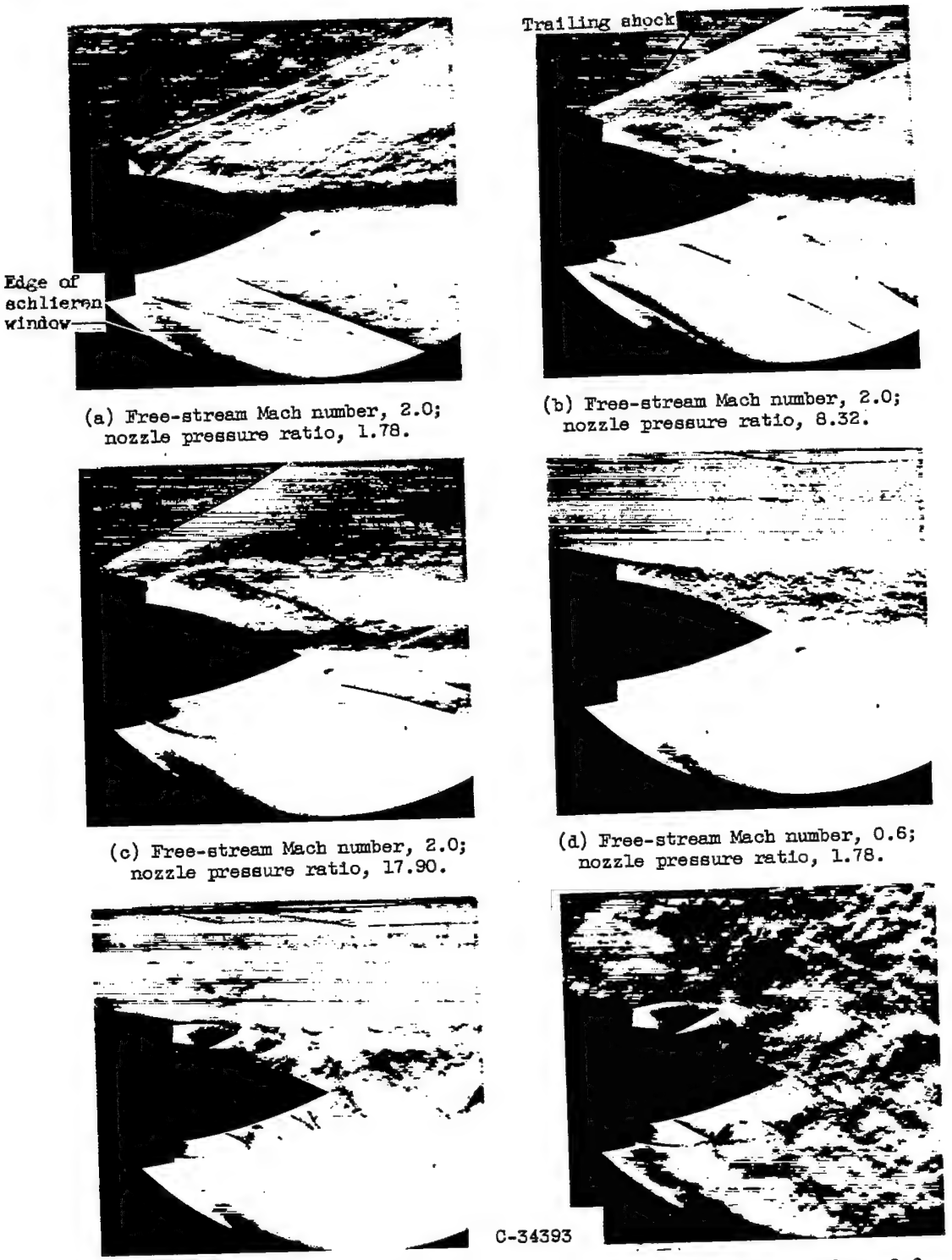

(a) Free-stream Mach number, 2.0; nozzle pressure ratio, 1.78.

(b) Free-stream Mach number, 2.0; nozzle pressure ratio, 8.32.

(c) Free-stream Mach number, 2.0; nozzle pressure ratio, 17.90.

(d) Free-stream Mach number, 0.6; nozzle pressure ratio, 1.78.

(e) Free-stream Mach number, 0.6; nozzle pressure ratio, 3.59.

(f) Free-stream Mach number, 0.6; nozzle pressure ratio, 5.39.

Figure 15. - Schlieren photographs of exhaust jet for convergent plug position at free-stream Mach numbers of 2.0 and 0.6 and [illegible] angle of attack.

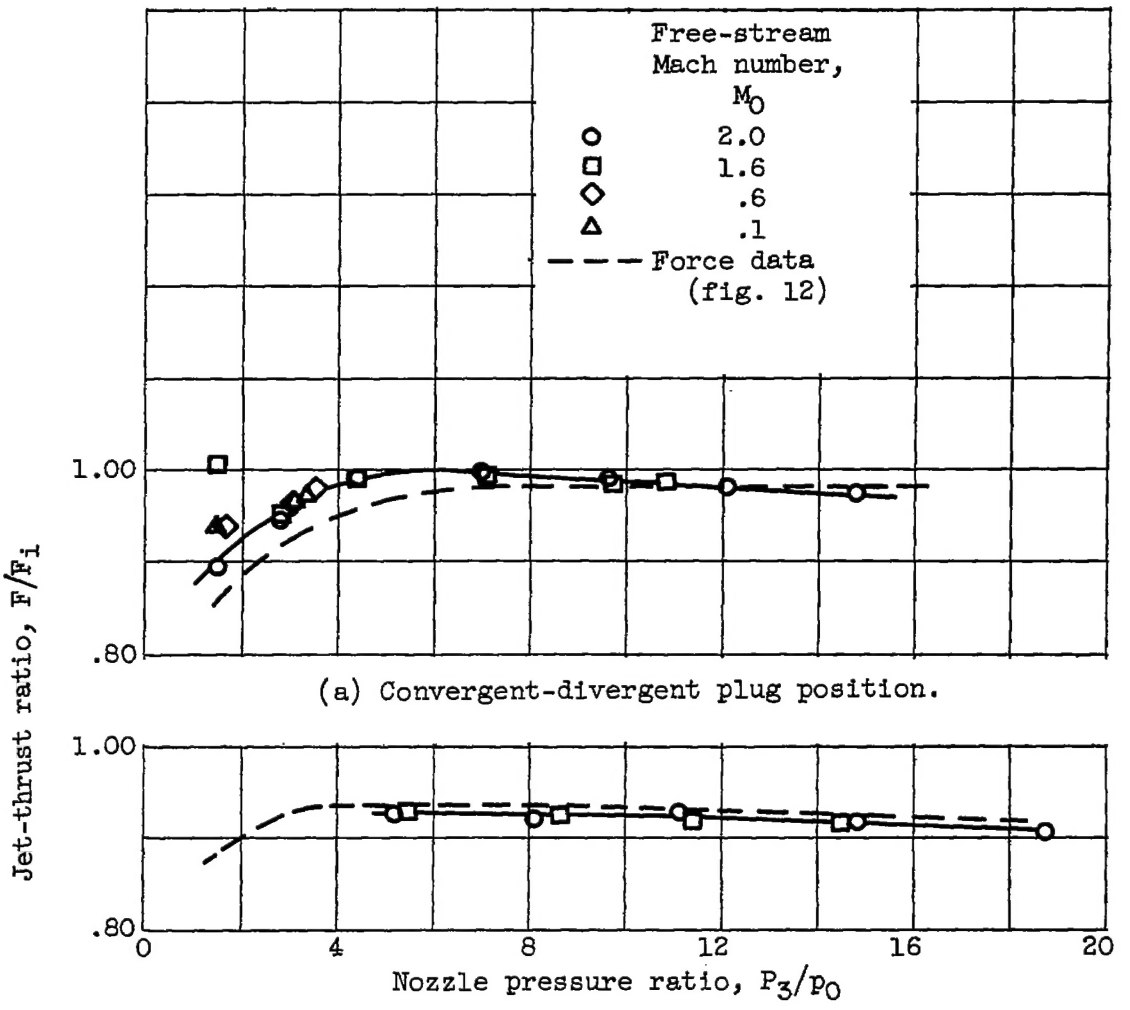

Figure 16. - Variation of jet-thrust ratio as obtained from pressure integration with nozzle pressure ratio.

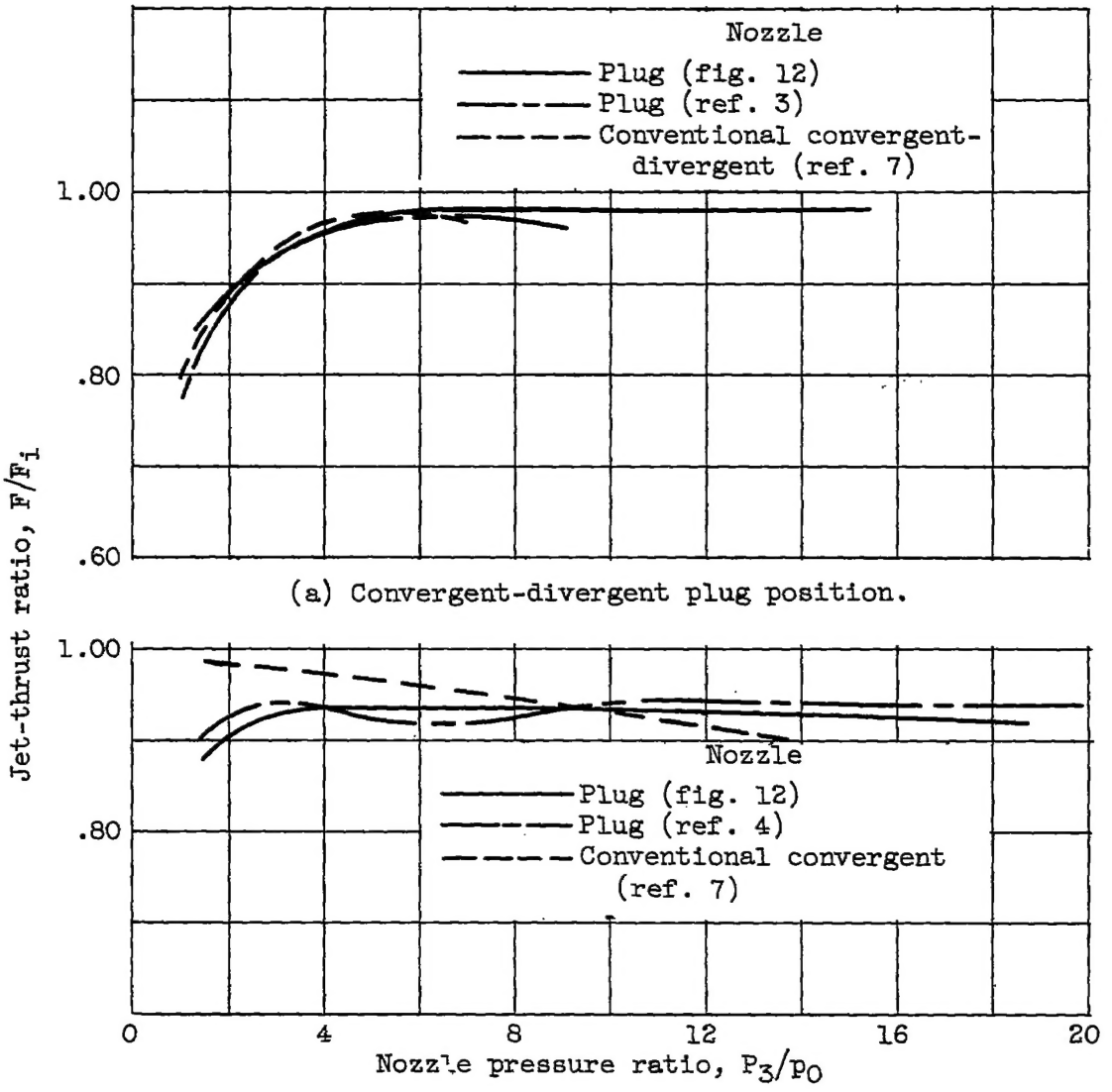

(a) Convergent-divergent plug position.

(b) Convergent plug position.

Figure 17. - Jet-thrust-ratio comparison with comparable plug and conventional-type nozzles investigated in quiescent air.

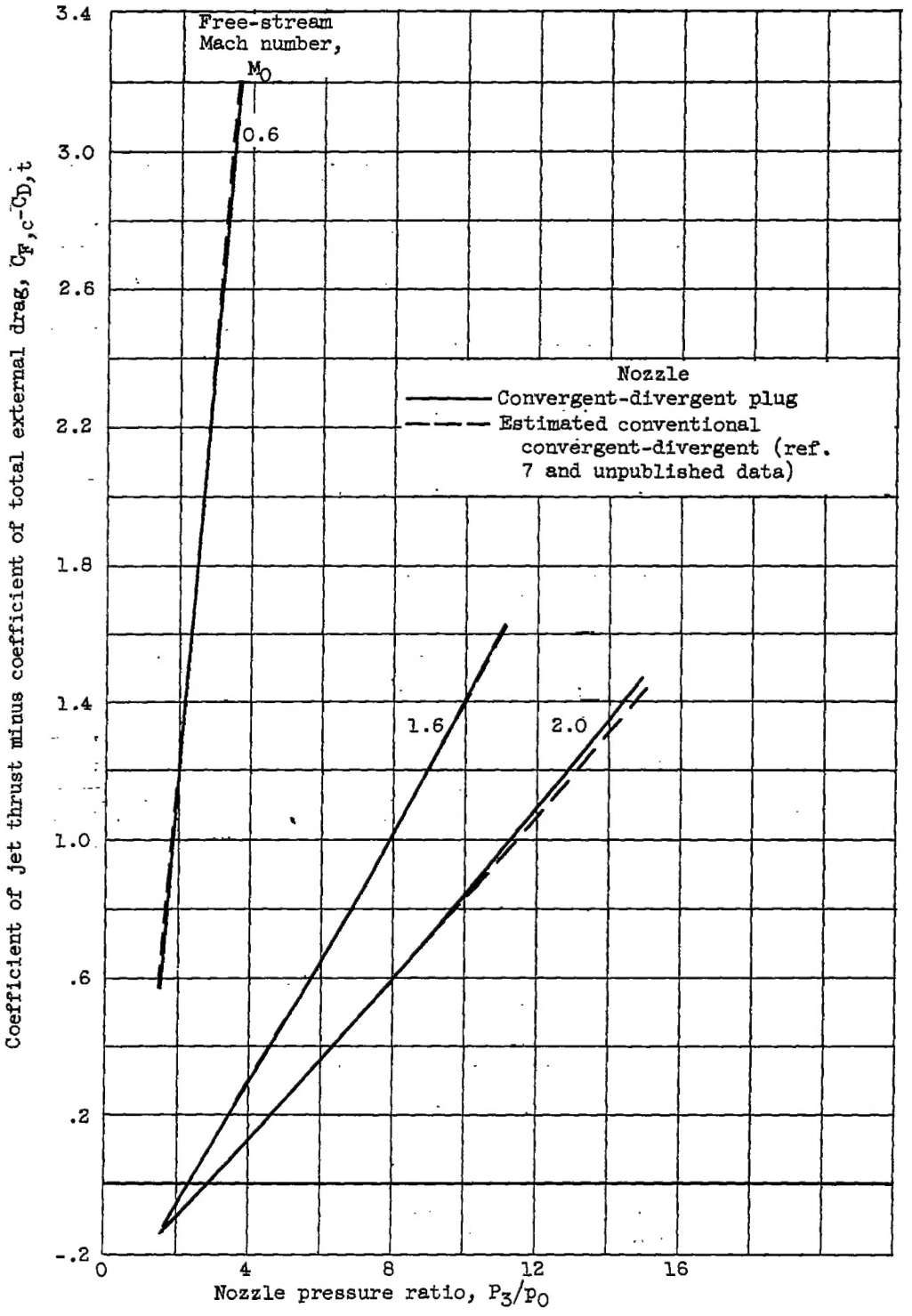

(a) Convergent-divergent plug position.

Figure 18. - Jet-thrust-minus-external-drag comparison.

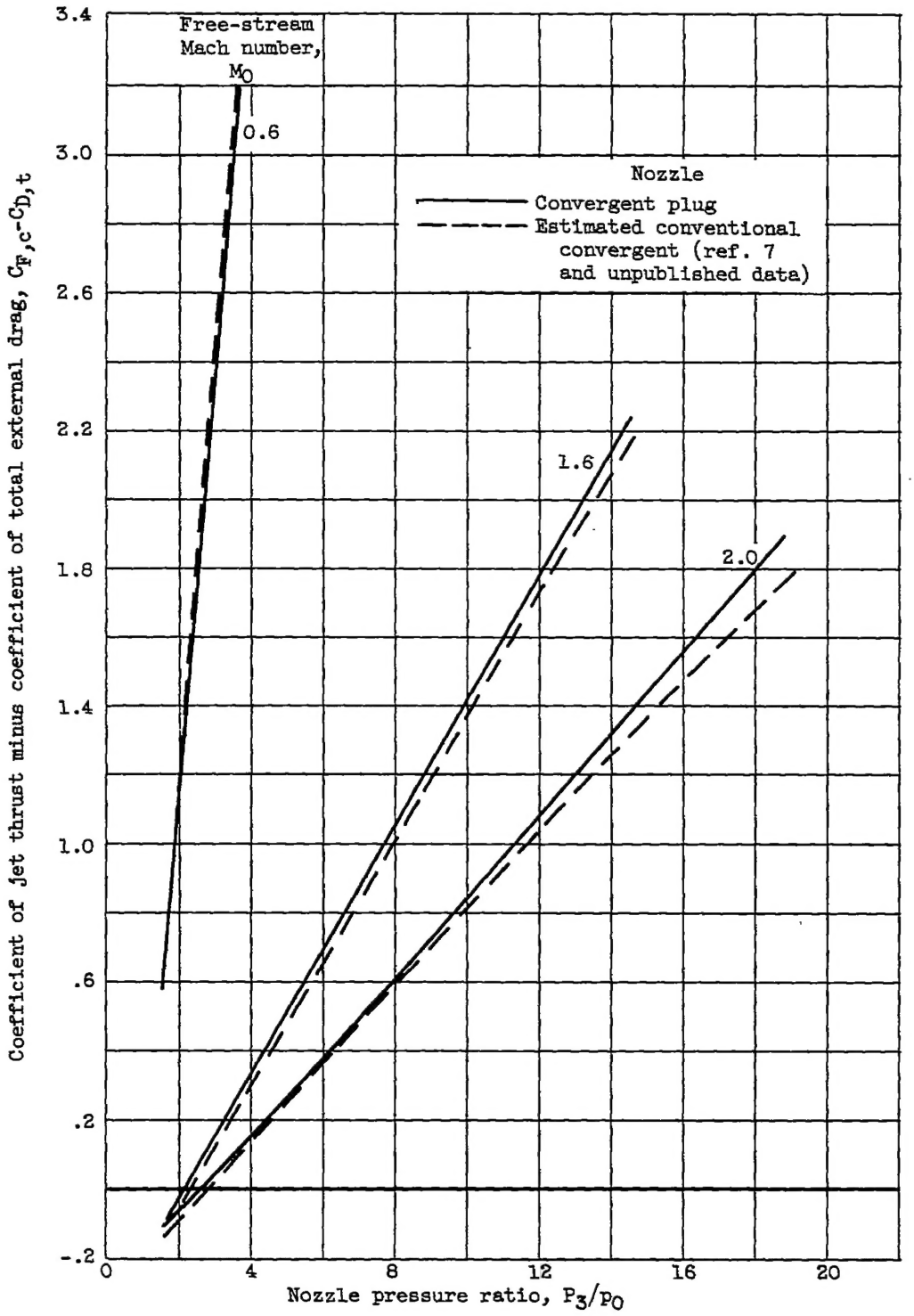

(b) Convergent plug position.

Figure 18. - Concluded. Jet-thrust-minus-external-drag comparison.

NACA-Langley - 2-19-54 - 325